J. Fluid Mech. (1984), *vol.* 146, *pp.* 383–415
Printed in Great Britain

Wake-induced galloping of two interfering circular cylinders

By A. BOKAIAN†
Earl and Wright Ltd, Consulting Engineers, Victoria Station House, 191 Victoria Street, London SW1E 5NE
AND F. GEOOLA
Department of Civil Engineering, University College London, Gower Street, London WC1E 6BT

(Received 8 December 1983 and in revised form 9 May 1984)

Measurements are presented of fluid-dynamic instability of a smooth circular cylinder, free to oscillate laterally against linear springs in the wake from an identical stationary neighbouring body. The observations also encompassed determination of static forces on the downstream cylinder as functions of relative position of the cylinder pair. Most of the experiments were performed under two conditions of free-stream turbulence. Static tests indicated that both the drag coefficient and the Strouhal number of the downstream body are continuous functions of its relative position. The drag forces were found to be negative at small gaps. It was observed that the transverse extent of the force field increases with increasing streamwise gap.

In the dynamic experiments, depending on the cylinders' separation and structural damping, the cylinder exhibited a vortex-resonance, or a galloping, or a combined vortex-resonance and galloping, or a separated vortex-resonance and galloping. Whilst the characteristics of wake-excited motion were found to be essentially unaffected by a limited change in free-stream turbulence intensity, the galloping amplitudes were observed to be sensitive to the cylinders' aspect ratio. An increase in the stability parameter caused significant effects on the cylinder response in amplitude domain. Wake observations behind the oscillating body indicated that in vortex lock-in the frequency of vortex-shedding locked to vibration frequency, but during small-amplitude galloping motion the shedding frequency behaved as if the cylinder was stationary.

1. Introduction

When a group of cylinders, such as the structural members of an offshore platform or a group of risers and tethers on a tension-leg platform, is exposed to fluid flow, downstream cylinders may be affected by the wakes of those further upstream. They may be subject to reduced mean velocities but greater turbulence, or they may be within enhanced velocity fields created by nearby cylinders. One approach to the problem of predicting the flow around such closely spaced members, and the resulting fluid-elastic instabilities, is to develop an understanding of interactions between flows by experiments on relatively simple arrangements of bluff bodies. In this paper we examine the phenomena associated with transverse vibrations of a rigid smooth circular cylinder, mounted on elastic supports and excited by the wake generated by a fixed identical parallel neighbour; the motion of the former being restricted to a plane perpendicular to the free-stream flow.

† Formerly at London Centre for Marine Technology.

It is an acknowledged fact that elastic cylindrical bodies in the wakes of other cylinders do not conform to the pattern of behaviour recorded when the cylinders are isolated. *Ad hoc* tests on proposed arrangements, by means of aeroelastic models in wind tunnels, have resulted in few generally applicable criteria; the complexity of the problem is emphasized by considering the large numbers of variables involved: e.g. spacings (in-line and across-flow), diameters, natural frequencies, elastic couplings and hysteretic damping between components in an array. Various modes of vibration associated with a cylinder pair have been studied experimentally by Roberts (1966), Cooper & Wardlaw (1971), Tanida, Okajima & Watanabe (1973), Price (1975), King & Johns (1976), Jendrzejczyk, Chen & Wambsganss (1979), Zdravkovich (1974, 1982) and Ruscheweyh (1983), amongst others. Additional references in the subject area can be found in Blevins (1979) and also in Zdravkovich (1977).

Zdravkovich (1974) carried out some very limited but interesting experiments in an open-circuit wind tunnel on the fluid-elastic instabilities of two identical rigid circular cylinders in a tandem arrangement (the line connecting the cylinder centres being parallel to the flow direction) over a Reynolds-number range from about 1×10^5 to 2×10^5 (based on the mean free-stream velocity and the diameter of an isolated cylinder). Amongst other arrangements, he held the upstream cylinder stationary while allowing the downstream one to have only a cross-flow vibration. This arrangement produced a large-amplitude low-frequency sinusoidal oscillation for all gap-to-diameter ratios up to 2.5. For values greater than this, an abrupt reduction in amplitude occurred of more than 10:1. These vibrations were random with no distinct frequency, and continued so up to the largest separation tested, corresponding to gap-to-diameter ratio of 6. The experimental results of this investigation, obtained under laboratory conditions, also indicate that under certain conditions and with the downstream cylinder well submerged in the wake of the upstream one, the rear (downstream) body may be subjected to large-amplitude oscillations induced by the turbulent wake of the front (upstream) body. The fluid-elastic instability is characterized by a vigorous build-up of oscillation amplitudes with increasing flow speed, for all flow speeds greater than a critical threshold flow velocity. This large-amplitude single degree of freedom oscillation was observed to be in many respects reminiscent of galloping of isolated non-circular cylinders, and for this reason it is referred to as 'wake-induced galloping'. The vibrations generally become more severe as the two bodies are brought closer together. However, once the gap between the two bodies exceeds a few diameters, the cylinder is not prone to galloping any more, and consequently the oscillation amplitudes drop considerably; the cylinder exhibits only a vortex-resonance excitation. The most fascinating feature of the wake-excited galloping is that both the mean position of the oscillation and the body's vibration frequency can vary appreciably with increasing flow speed.

The wake-induced galloping mentioned above must not be confused with 'wake-excited flutter' and so on frequently encountered in overhead power lines (Cooper & Wardlaw 1971; Simpson 1971; Price 1975). Flutter involves, by necessity, the participation of at least two degrees of freedom. Galloping, on the other hand, carries the strong connotation of a negatively damped single degree of freedom oscillation, and its use to describe the problem under study is only because of the many similarities between the two kinds of instability.

The aim of the present investigation is to examine experimentally the fluid-elastic instability of a circular cylinder, both in amplitude and frequency domain, immersed in the wake of a fixed parallel neighbour for a range of relative positions, governing flow and structural parameters. It is designed to study some of the characteristics

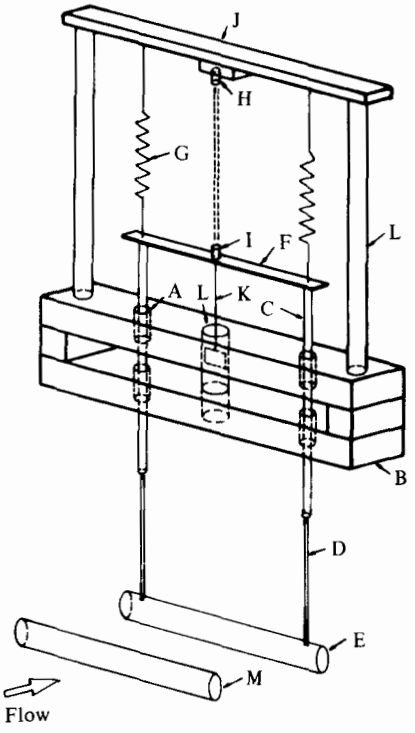

FIGURE 1. Sketch of the dynamic test apparatus: A, air bearing; B, air-bearing housing; C, air-bearing shaft; D, arm; E, vibrating cylinder; F, cross-bar; G, spring; H, receiving transducer; I, transmitting transducer; J, rigid frame; K, damper connecting shaft; L, oil pot; M, stationary cylinder.

of the wake-induced instability and to define the region of the wake within which this phenomenon may occur. Also presented are the measurements of the lift and drag forces of the downstream cylinder at various Reynolds numbers and under different free-stream turbulence conditions. Observations of the vortex shedding behind the vibrating body are discussed.

2. Experimental equipment and procedure

All the experiments were conducted in an open channel in the Department of Civil Engineering at Imperial College, London. The water channel had a rectangular cross-section 0.3 m wide and 0.3 m high, with a horizontal smooth aluminium bed and vertical glass sidewalls. The overall length of the channel, from the end of the contraction to the downstream gate, was 18 m long. A layer of gravel baffles together with a thick layer of rubberized horsehair baffle was positioned across the settling chamber near the pipe outlet in order to improve the uniformity of the mean velocity across the channel and also to help dissipate disturbances in the flow after it left the pipe outlet. In addition, a series of specially designed turbulence-reducing screens with a separation of 10 cm was installed in the settling chamber just before the leading streamlined plates of the flume.

A fundamental study of the dynamic response of a circular body in a wake flow could be made using a two-dimensional spring-mounted model, the general layout of which is shown in figure 1. This apparatus was basically symmetrical with respect to the flume (channel) centreplane. The vibrating cylinder was held horizontally in

the flume by two identical very thin arms of width 6 mm; the two arms being separated by a horizontal distance of 250 mm. Each arm was attached to a shaft and each shaft in turn passed through a pair of air bearings. The four air bearings were embedded symmetrically in a housing consisting of two blocks of dural. The upper ends of the two vertical shafts were connected together by means of a very light horizontal cross-bar, and the whole system was suspended from a rigid frame by means of two identical helical springs, each with a stiffness of 8.53 N/m. The air-bearing housing was bolted to a rigid dural girder construction, mounted on rollers permitting easy movement along the flume rails. Provision was made for very fine adjustments of the girder in every direction to ensure that the cylinder could be aligned parallel to the flume bed with its frontal side facing the approaching water flow.

Owing to high air pressure in the bearings, the vibrating system had a purely cross-flow movement with a minimum viscous structural damping. The effect of increased structural damping on the cylinder vibrations could be studied by artificially applying an external damping to the system. This was done by means of a very thin vertical plate immersed in an oil pot and connected to the cross-bar by means of a very slender shaft; the oil pot being placed in the two dural blocks. The effect of increased modal mass on the vibrations could be investigated by placing additive masses on the cross-bar.

To detect the system movement, an ultrasonic displacement-measuring device connected to the cross-bar was used. This device essentially consisted of a pair of transducers, one transmitting and the other one receiving. The transmitter was attached to the moving body whilst the receiving one was fixed to the frame. This non-touching instrument was coupled with an ultraviolet recorder to obtain a permanent trace of the response of the system.

Prior to the experiments, the dynamic testing equipment was adjusted so that the cylinder position in still water was halfway between the flume bed and the free water surface. The end gaps between the model and the glass sidewalls were 1 mm. The front cylinder was similarly held horizontally in the flume, parallel to the rear one, by two identical very thin but rigid arms connected to a mechanical device. With the aid of this device, the upstream model was able to traverse in either the transverse or streamwise directions. Whereas the rear cylinder had a free oscillation, the front one was rigidly constrained. There was practically no end gap between the upstream model and the flume sidewalls. The relative displacement between the front cylinder and the mean position of the rear one was measured by means of a transducer.

To measure the mean fluid-dynamic forces on a cylinder immersed in the wake of a similar cylinder, the two bodies were held vertically, with the rear cylinder always being held in the centreplane of the flume. The downstream cylinder was supported by a cone-and-socket device, with the cone resting on the flume bed and the socket being fixed to the cylinder lower end. To remove the free-water-surface effects, the working section was roofed over with a horizontal perspex plate of $2 \times 20 \times 100$ cm, as sketched in figure 2. Through a tiny hole in the roof, the rear cylinder was mounted at the top to a unidirectional force transducer fixed to a horizontal turntable. The base plate of the turntable was supported by the flume rails. The roof was provided with a mesh of tiny holes corresponding to the locations of the upstream cylinder. Whereas the front body spanned the full height of the working section, there were small end-gaps between the rear body and the two horizontal boundaries. The force was inferred by measuring the displacement of the upper end of the cylinder by means of a Commodore minicomputer via an analog–digital converter and using a force displacement calibration curve.

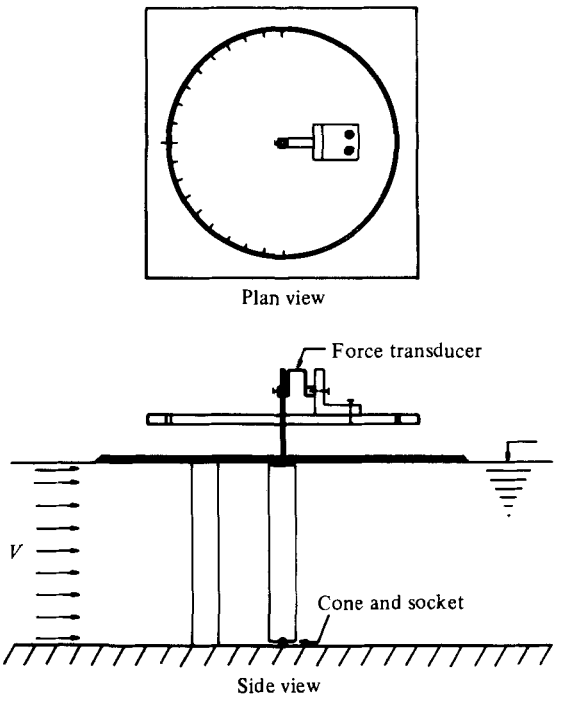

FIGURE 2. Schematic representation of the apparatus designed to measure the drag and lift forces on downstream cylinder.

A Pitot–static tube or a miniature current flowmeter was used for time mean velocity measurements. The velocity fluctuations in the free stream and in the neighbourhood of the cylinder pair were detected with a TSI linearized constant-temperature-type hot-film anemometer. The output of the hot film was fed into a combined analog–digital converter and the minicomputer.

3. Test programme

The working section was situated at a distance of about 1 m from the leading streamlined plates of the channel. Throughout the experiments, the water depth at this section was kept constant at roughly 290 mm. At this depth, the channel could have a maximum average flow speed of 70 cm/s. It was feared that the proximity of the settling chamber to the test station could seriously affect the velocity distribution at this section. For this reason, with the aid of the Pitot–static tube, measurements were made of the velocity distribution at various discharges. A vertical profile taken at the centre of the channel is shown in figure 3(*a*), where the local velocity V_1, non-dimensionalized by the average velocity V (defined as the discharge divided by the cross-sectional area of the flow), is plotted against y_1/H, where y_1 is the distance from the bottom of the channel and H is the water depth. This profile is for the average velocity $V = 26$ cm/s. A profile across the channel, taken at about half the water depth and for $V = 25.8$ cm/s, is indicated in figure 3(*b*), where z_1 is the distance from one wall and W is the width of the channel.

The relative uncertainty in measuring the velocity at any point was about 1.5%, and therefore much of the scatter in figure 3 can be attributed to measurement error. This figure shows a reduction in the velocity towards the free surface, where the measurements showed some unsteadiness due to the cross-waves generated in the

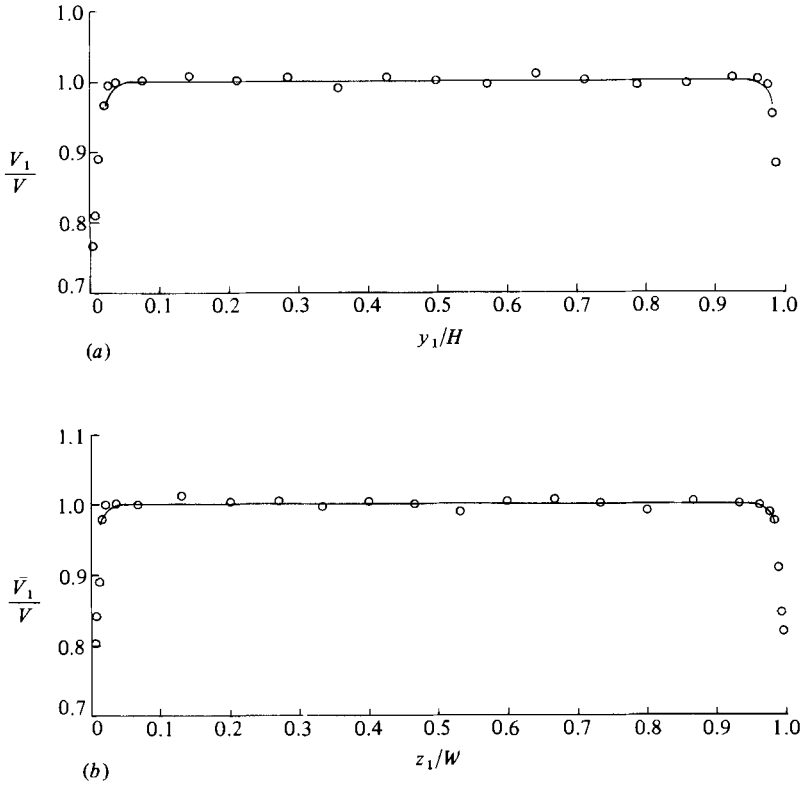

FIGURE 3. Mean-velocity profiles at the working section: (*a*) vertical profile for $V = 26$ cm/s; (*b*) transverse profile for $V = 25.8$ cm/s.

settling chamber and in the channel. Considering that the measurements very close to the bed and the sidewalls are inaccurate, one may conclude that the velocity field at the working section was uniform over a major portion of the section, with the boundary-layer thickness being less than 6 mm.

The hot-film probe was employed to identify the turbulence characteristics at the test station, namely the scale and the intensity. The background turbulence at the working section had intensity $(\overline{v^2})^{\frac{1}{2}}/V = 6.5\,\%$, where v and V represent the streamwise fluctuating velocity and the time-mean free-stream velocity respectively. The average value of the associated integral lengthscale was 16 mm. This indicates that although several meshes in the settling chamber were successful at improving the mean-velocity distribution, they were not suitable for reducing turbulence.

To find out the effects of the increase in turbulence intensity on the flow around the cylinder pair and the related flow-induced vibrations, a square-mesh grid was installed at a distance of 360 mm upstream of the test station. The grid, which was biplanar, was constructed with bars of circular cross-section of 16 mm diameter and a mesh-to-bar ratio of 5 : 1. The associated turbulence intensity and integral lengthscale were on average 11.9 % and 8 mm respectively. The water channel was used in two different configurations, either with or without the turbulence grid. In both cases the turbulence was found to be roughly homogeneous at the test station, and the intensity and scale changed only slightly with increasing the mean velocity.

Four different models were tested. They comprised two pairs of circular cylinders of 8 mm and 16 mm diameter. The cylinders were made of PVC, and had a smooth surface.

The addition of free-stream turbulence reduces the critical Reynolds number R_c for an isolated circular cylinder. However, for a cylinder of 16 mm diameter, some calculation based on the method of Kiya *et al.* (1982) showed that the values of R_c were about 5.6×10^4 and 3.2×10^4 in 6.5% and 11.9% turbulent flow respectively. These two values are considerably higher than the maximum Reynolds number (based on the diameter of an isolated cylinder) used for the measurements. Therefore it is expected that the cylinder flow was within the subcritical regime in all tests.

The experiments carried out with the pair of identical cylinders can be broadly classified into two series: (1) tests to determine the static forces on the downstream body; and (2) dynamic tests to investigate the cross-flow response of the rear cylinder as a function of streamwise and lateral spacing between the centre of the upstream body and that of the downstream one in its mean position, and also the sensitivity study of the influence of parameters such as structural damping and mass ratio on the behaviour of the vibrating cylinder. The separation between cylinder centres was varied from 1 to 5 cylinder diameters longitudinally and zero to 3 diameters laterally. Most of the experiments were to be done for two levels of free-stream turbulence. All the measurements were carried out in the same water channel position, thereby eliminating any differences due to water-channel characteristics.

A single cylinder of 16 mm diameter occupied about 5% of the area of the channel working section. With two cylinders in the channel, at certain separations, marked flow asymmetry was found, and it was not thought possible to correct accurately for the effects of blockage. Therefore the results are presented uncorrected.

4. Experiments and experimental results

4.1. *Strouhal number of the downstream cylinder*

The shedding frequency behind the downstream member of a stationary cylinder pair is presented non-dimensionally in the form of the Strouhal number $S_2 = f_s D/V$, where f_s and D are the vortex-shedding frequency and the cylinder diameter respectively. Figure 4 summarizes the variation of S_2 as a function of the relative position of the cylinder pair. In this figure x_0 and y_0 are defined as the longitudinal and transverse spacings between the centres of the cylinders divided by D, while Re denotes the free-stream Reynolds number (based on the diameter of a single cylinder). These results are taken from previous work of the authors (Bokaian & Geoola 1984*b*). As reported in the same paper, in tandem arrangement, the vortex shedding behind the upstream body was suppressed up to two diameters separation. Despite this, no discontinuity can be seen in the variation of S_2 in relation to the cylinders' spacing.

4.2. *Static lift and drag forces*

A variety of measurements of lift and drag forces on a circular cylinder submerged in the wake of an identical parallel neighbour have been reported by various researchers at different Reynolds numbers (Wardlaw & Cooper 1973; Cooper 1974; Price 1975). In this work a set of two circular cylinders of 16 mm diameter was used for the static-force observations. The measurements were carried out at seven streamwise stations with separations of 1.09, 1.5, 2, 2.5, 3, 4 and 5 diameters. At each station the forces were explored for roughly 20 transverse locations in one side of the flume centreplane (positive lateral spacing). Occasionally some measurements were made in the other side of the flume. The lift and drag coefficients C_L and C_D were calculated by dividing the hydrodynamic force values by the product of the free-stream dynamic pressure times the projected area of the cylinder, i.e. $\frac{1}{2}\rho V^2 DL$, where ρ is the fluid density and L is the cylinder length. Owing to non-uniformity of the

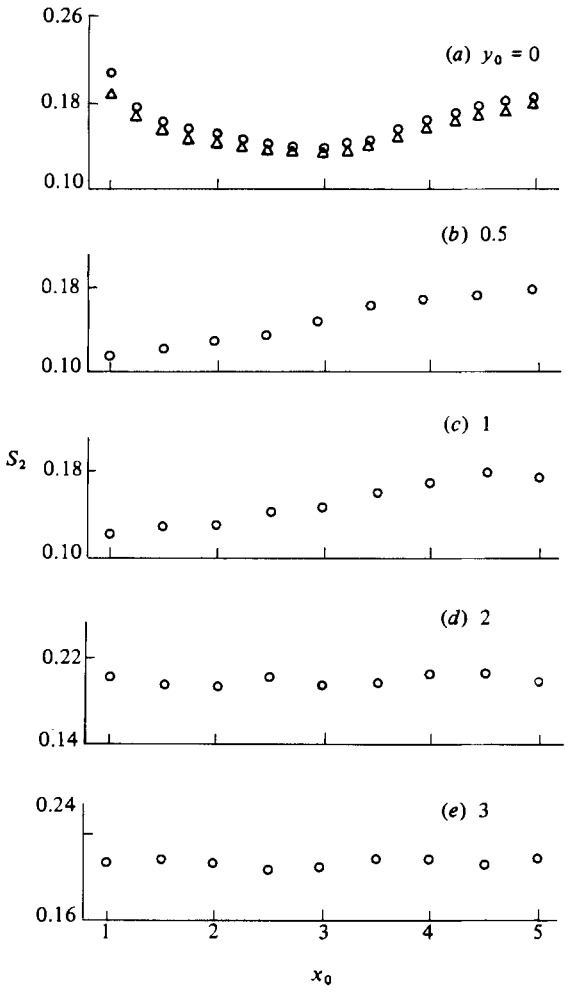

FIGURE 4. Variation of the Strouhal number of the downstream cylinder (fixed) as a function of streamwise and transverse separation ratio (Bokaian & Geoola 1984*b*); $L = 300$ mm, $D = 16$ mm, $(\overline{v^2})^{\frac{1}{2}}/V = 6.5\%$: ○, $Re = 5.6 \times 10^3$; △, $Re = 1.15 \times 10^3$.

approaching flow, a correction (Price 1976) had to be made to the force measurements, though this correction was found to be inappreciable.

The water-channel tests were performed at two values of free-stream velocity corresponding to $Re = 2900$ and 5900. In the experiments associated with the higher Reynolds number, the observations were conducted under the two conditions of free-stream turbulence. The rear cylinder was removed when measuring the drag force on an isolated cylinder. This procedure led to single-cylinder drag values of $C_{D\infty} = 1.26$ and 1.25 in a water flow with 6.5% turbulence level at $Re = 2900$ and 5900 respectively. With an increase in turbulence intensity to 11.9%, the single-cylinder drag fell to 1.17 at $Re = 5900$ and to 1.19 at $Re = 2600$.

Indicated in figure 5 are the measured values of the drag coefficient as a function of transverse position in the wake of the upstream cylinder. For the sake of clarity, a smooth curve was drawn through the measurements associated with the higher Reynolds number ($Re = 5900$) at the 6.5% turbulence level. Figure 5 clearly demonstrates that the variation of drag coefficient is symmetrical about the wake centreline and also has a minimum value C_{D0} on this line.

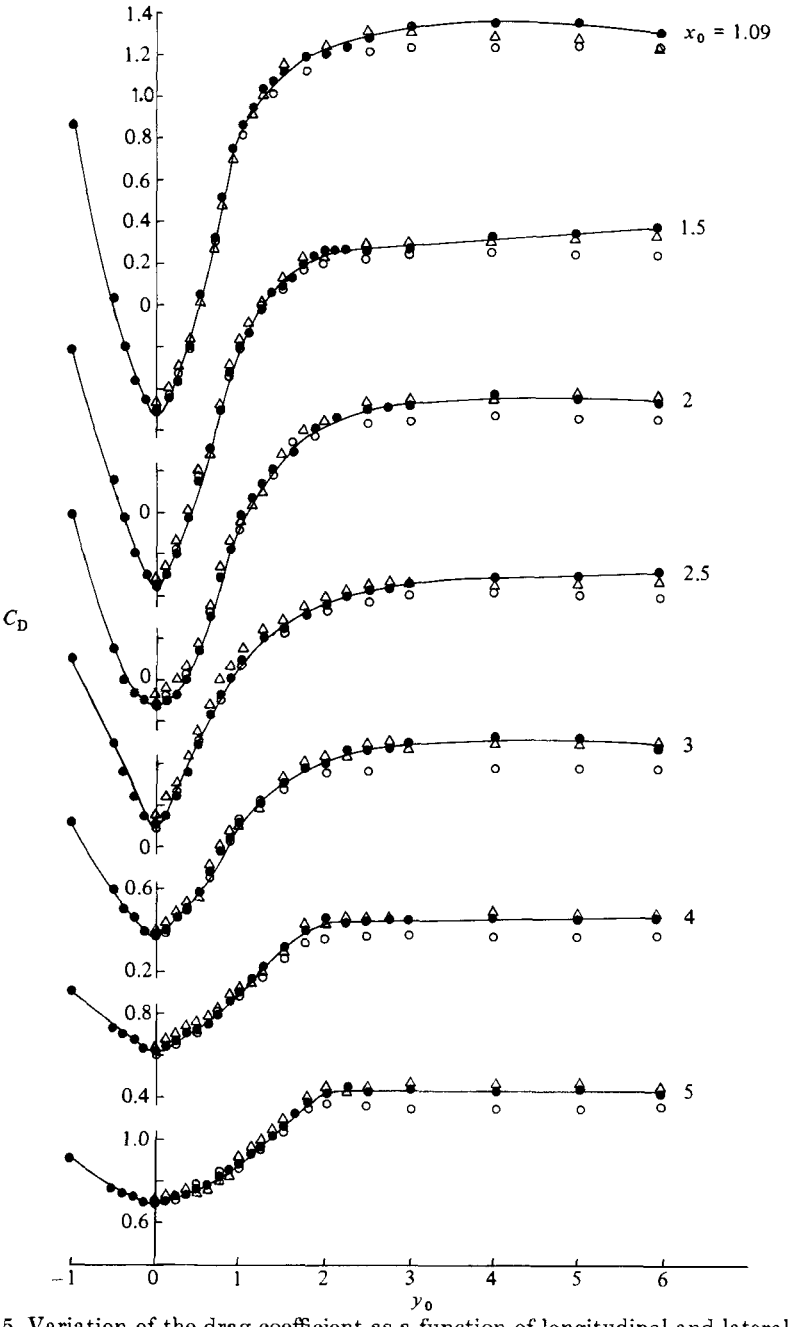

FIGURE 5. Variation of the drag coefficient as a function of longitudinal and lateral spacing ratio: ●, Re = 5900, $(\overline{v^2})^{\frac{1}{2}}/V$ = 6.5%; △, 2600, 6.5%; ○, 5900, 11.9%.

A notable feature of the distribution of the drag coefficient is that it is insensitive to a limited increase in Reynolds number from Re = 2600 to 5900. A similar conclusion was drawn by Price (1975) for a Reynolds-number range one order of magnitude greater than those of the present work. However, for a fivefold increase in Reynolds number, Wardlaw & Cooper (1973) and Cooper (1974) observed a small change in drag-coefficient profiles for separations less than 4 diameters, while discovering a considerable change for larger spacings. Contrary to that, the effect of

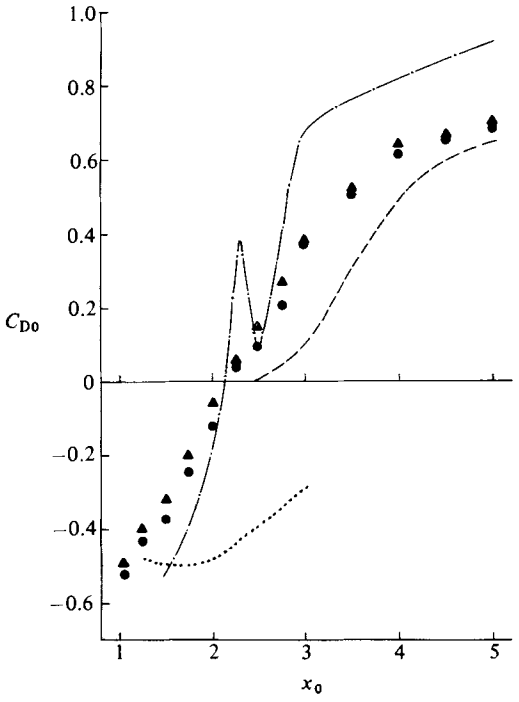

FIGURE 6. Variation of the drag coefficient in tandem arrangement against the longitudinal spacing ratio. Present study $(\overline{v^2})^{\frac{1}{2}}/V = 6.5\,\%$): ●, $Re = 5900$; ▲, $Re = 2600$. Tanida *et al.* (1973): ——, $Re = 3400$, $((\overline{v^2})^{\frac{1}{2}}/V = 0.1\,\%$. Kostic & Oka (1972): —·—·—, $Re = 13000$, $(\overline{v^2})^{\frac{1}{2}}/V = 2.8\,\%$. Hori (1959): ·····, $Re = 8000$, $(\overline{v^2})^{\frac{1}{2}}/V = ?$.

turbulence on the lateral variation of drag coefficient is seen to be profound, and becomes quite noticeable when the transverse distance between the adjacent sides of two cylinders is greater than one diameter. It is notable to mention that Price observed an increase in minimum drag coefficient when he increased the turbulence intensity from 1.5 % to 11.5 %. Moreover he concluded that the increase in turbulence causes the profiles to decay at less distance between cylinders.

Figure 6 shows the variation of minimum drag C_{D0} versus the separation ratio x_0. Also shown in this figure are the data reported by previous workers having Reynolds numbers close to those of the present study. They comprise the results of Hori (1959) measured in a wind tunnel at a Reynolds number of $Re = 8000$ (with unspecific characteristics), Kostic & Oka (1972) obtained by integrating the pressure distribution around the circumference of the cylinder in a uniform turbulent flow of a wind tunnel with the intensity of 2.8 % at $Re = 13000$, and those of Tanida *et al.* (1973) measured by towing two cylinders in a water tank at $Re = 3400$. The results of the present investigation indicate a continuous variation of C_{D0} against the cylinders separation, which is in accord with the fact that there is no discontinuity in the variation of the Strouhal number S_2 versus the spacing. Wide differences between the various data in figure 6 can be attributed to the techniques used to measure the force (integration of pressure distribution, balance, strain gauge, etc.), and the errors involved, as well as the individual or collective effects of Reynolds number, turbulence characteristics and the cylinders' aspect ratio.

The data points of the lift coefficient, as a function of x_0 and y_0, are similarly shown in figure 7. In plotting this figure the positive direction of the lift force was assumed

to be towards the centre of the wake. A smooth curve was again drawn through the data with 6.5 % turbulence level and a Reynolds number of $Re = 5900$. This figure indicates that the lift forces were approximately zero when the two cylinders were aligned longitudinally. From the observations in figure 7 it is clear that the lift coefficient is essentially unaffected by a limited increase in Reynolds number. A similar conclusion was reached by Price (1975), although Wardlaw & Cooper (1973) and Cooper (1974) observed a slight change in lift-coefficient profiles with increasing Reynolds number.

From a comparison of the tests carried out in flows with different free-stream turbulence characteristics, it is concluded that the lift-force field is insensitive to a limited increase in turbulence intensity. However, Price (1975) found that by increasing the turbulence intensity from 1.5 % to 11 % the maximum lift coefficient was reduced and was also moved in towards the centre of the wake, with the value of $\partial C_{\mathrm{L}}/\partial y_0$ remaining roughly equal in the central region.

Figure 8 indicates the variation of the maximum lift coefficient $C_{\mathrm{L}\max}$ and the corresponding transverse separation ratio $y_{\max}$ against the relative streamwise position x_0. As can be seen in this figure, the magnitude of $C_{\mathrm{L}\max}$ continually decreases on increasing the longitudinal spacing, but the transverse extent of the force field increases farther downstream as the wake widens.

4.3. *Dynamic-test results*

The procedure for dynamic testing was to set the front body at a fixed relative lateral separation y_0. Its position was then changed in the streamwise direction. A total number of 37 dynamic experiments were performed, the significant details of which are given in table 1. Columns (1), (2) and (3) represent the run number and the corresponding spacing ratio x_0 and y_0 respectively. These two quantities are respectively the relative along-flow and across-flow spacings between the centre of the upstream cylinder and that of the downstream one in its undisturbed position.

At the test outset the natural circular frequency ω_{n} of the system in still water was determined from the transient decay traces of the system in still water. The extinction test involved recording motion on the UV recorder when the cross-bar was displaced from the equilibrium position. The initial displacement Y_0 to the system relative to the mean position in still water was about 50 mm. Indicated at the bottom of table 1 is the relative initial displacement, which was 6.26 in run T1*b* and 3.13 in other tests. The half-cycle peak amplitude and the half-cycle durations were measured from the stripchart recording of the oscillatory response. To within the accuracy of the measurements (errors of the order of 1 %), the half-cycle duration was found to be constant. This means that, in spite of the proximity of the oscillating cylinder to a fixed identical body, the response frequency in still water, and hence the total vibrating mass m (i.e. the mass of the system in still water plus the added mass of the cylinder), were constant and independent of the oscillation amplitude from $Y_0 \approx 50$ mm down to measurable limits of amplitude. The values of the natural frequency and the mass parameter $n = \rho D^2 L/2m$ are shown in columns (4) and (8) respectively. It can be seen that the experiments have almost the same value of natural frequency. The cylinder added mass was obtained by subtracting the measured mass of the system in still water from the total vibrating mass. Indicated in columns (5) and (6) respectively are the values of the vibratory Reynolds number $\gamma = \omega_{\mathrm{n}} D^2/\nu$ and the added-mass coefficient C_M. The value of C_M was calculated by dividing the measured added mass by the displaced mass of the fluid $\frac{1}{4}\rho\pi L D^2$. As can be seen in column (5), with the exception of test T1*b*, which had a value of $\gamma = 291$,

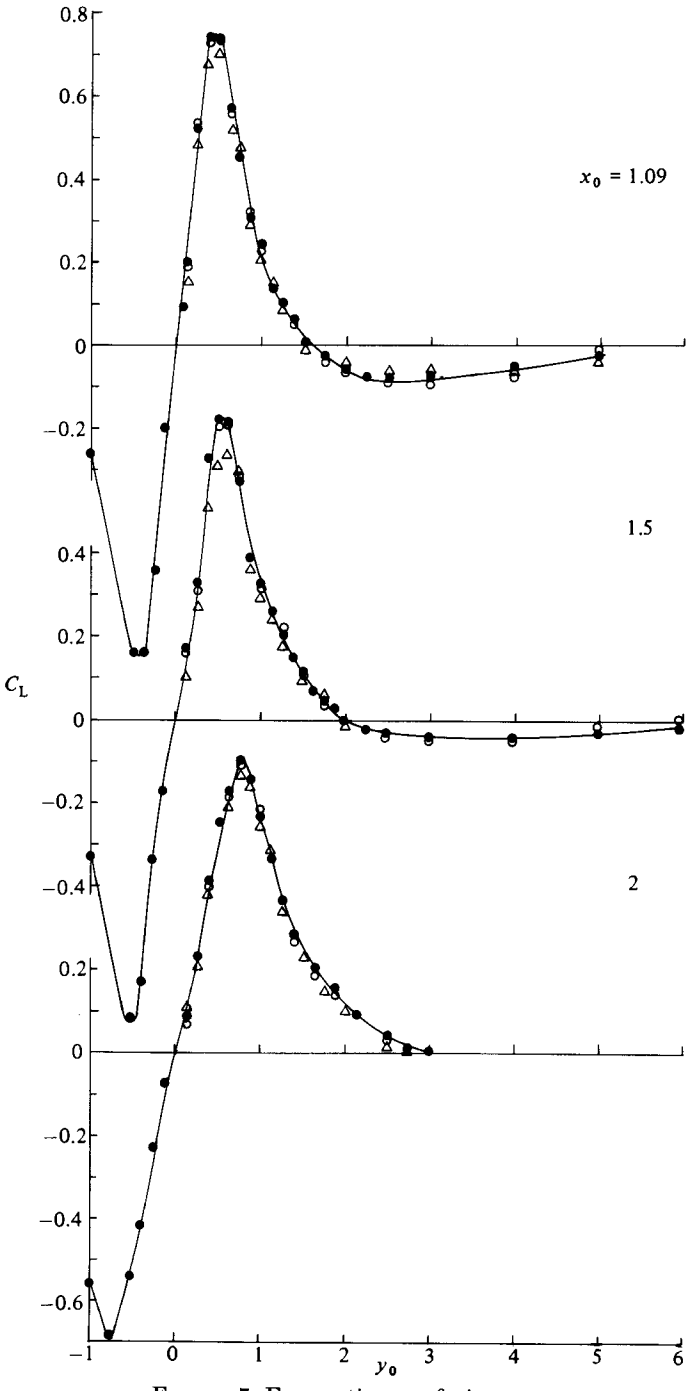

FIGURE 7. For caption see facing page.

the rest of the runs had a vibratory Reynolds number of about 1050, with the added-mass coefficient ranging from 1.67 to 1.70. In regard to added mass, it is known that the added mass of a body can be seriously affected by the presence of other neighbouring bodies (Chen, Wambsganss & Jendrzejczyk 1976; Yang & Moran 1979). However, the above observations surprisingly demonstrate that the still-fluid added

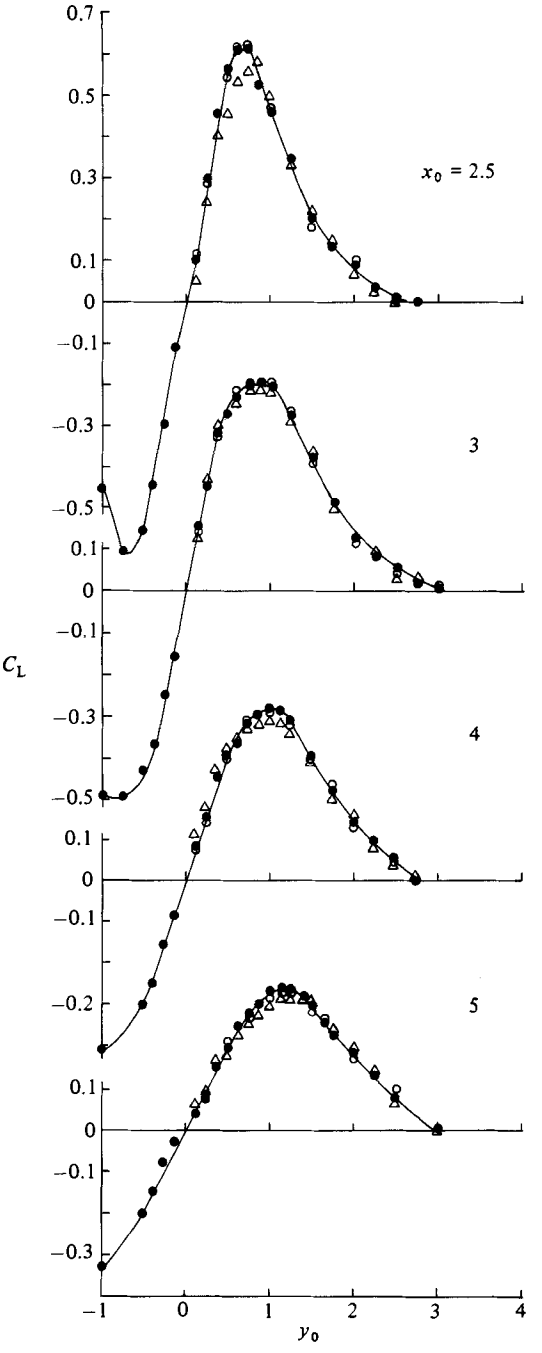

FIGURE 7. Variation of the lift coefficient C_L as a function of the longitudinal and lateral spacing ratio. Symbols as in figure 5.

mass of the oscillating cylinder was very little affected by its proximity to an identical fixed body, even when the gap between the two cylinders was very small. The added-mass coefficient of run T1*b* is considerably higher than those of the others. This may be because this experiment has a lower vibratory Reynolds number.

Next, the system's structural damping was evaluated by removing the cylinder

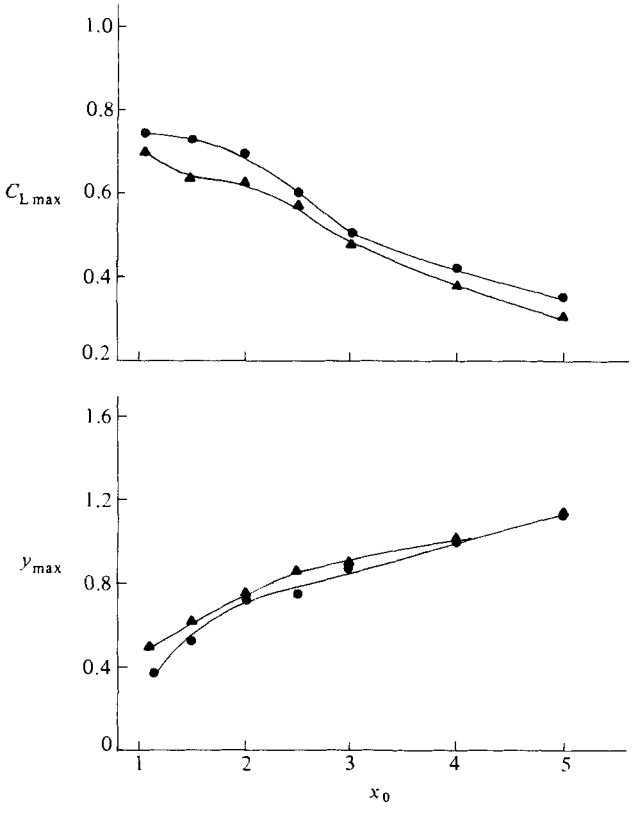

FIGURE 8. Variation of the maximum lift coefficient and the corresponding transverse spacing ratio as functions of relative streamwise separation; $(\overline{v^2})^{\frac{1}{2}}/V = 6.5\,\%$: ●, $Re = 5900$; ▲, $Re = 2600$.

from the arms and putting enough additive mass on the cross-bar so that the natural circular frequency of the system in still water would have a value equal to ω_n. The structural-damping coefficient c was deduced from recordings of logarithmic decrements in still water. The damping thus obtained was found to be viscous in all experiments. Column (7) indicates the values of the reduced damping $\beta = c/2m\omega_n$ of the tests. In each dynamic experiment, the values of the natural circular frequency ω_n, the reduced damping β and the mass parameter n of the oscillating system were fixed. Measurements were made of the free-stream flow speed V in the flume, together with a simultaneous recording of the vibration amplitude and frequency. The approximate range of the Reynolds numbers of the dynamic experiments is shown in column (11).

When studying the vortex-induced oscillation of bluff bodies, the vortex-resonance speed U_r becomes an important parameter. U_r can be written as $U_r = 1/2\pi S_2$, where S_2 is the Strouhal number of vortex-shedding behind the stationary downstream body (see figure 4). The values of U_r for the tests are shown in column (9). Column (10) indicates the values of the stability parameter $k_s = 2\pi\beta/n$ (Vickery & Watkins 1962) for the runs. Apart from experiments T1*a*, T2, T3, T4, T5, P1, P2, P3, P4, Q1, Q2 and Q3, which were conducted under two conditions of free-stream turbulence, the remainder of the tests were performed only in 6.5 % turbulence level.

The dynamic test data are summarized in figures 9–14 in a dimensionless form, with the reduced amplitude a defined as the oscillation amplitude divided by the cylinder

diameter, and the vibration frequency ratio $\Omega = \omega_c/\omega_n$, where ω_c is the system's response frequency, plotted against the reduced flow velocity $U = V/\omega_n D$. The short arrows along the U-axis indicate the vortex-resonance speed U_r. The reduced velocity was varied between approximately 0 and 6, usually by changing V and holding ω_n constant. In some experiments, the mean position of the cylinder, either when the body was stationary or vibrating, varied with changing free-stream flow speed. Measurements of the dimensionless mean position p, defined as cylinder mean position divided by D, are shown in the above figure plotted versus the reduced velocity. Although the results of this investigation indicate trends consistent with those of Zdravkovich (1974), no quantitative comparison could be made between the two. This is because, unfortunately, some of the vital information of Zdravkovich's observations are missing. It is quite clear in the above figures that an increase in free-stream turbulence intensity from 6.5% to 11.9% has no appreciable bearing on the results.

The above data indicate that, depending on the cylinders' spacing and mass and structural damping, the cylinder exhibited a vortex-resonance, or a galloping, or a combined vortex-resonance and galloping, or a separated vortex-resonance and galloping. Shown in the lower part of figure 15 is the type of instability that was observed at each spacing. 'a' refers to a vortex lock-in, whereas 'b', 'c' and 'd' denote respectively a galloping excitation, a combined vortex-resonance and galloping, and a separated vortex-resonance and galloping. As can be inferred from this figure, the behaviour of the vibrating body depends strongly on the relative position of the cylinder pair. Moreover, in wake-induced instability, depending on mass and structural damping, there can be more than one pattern at a given separation.

The experimental observations drawn in figures 9–13 have about the same stability parameter value, between 1.031 and 1.072. The results of tandem arrangement are indicated in the first figure. The vortex-resonance part of the data are shown magnified in figure 9(*a*). As figure 9 denotes, in tandem arrangement, the instability began in a small range of reduced velocities $0.6 < U < 0.75$. For the smallest gap between the two bodies (run T1*a* with $x_0 = 1.09$), the oscillation began at a reduced velocity of about 0.6 and has a galloping pattern. The vibration amplitude indicates a rapid increase with increasing flow speed until a reduced velocity of $U \approx 1.2$, beyond which the rate of increase declines. It seems that the oscillation amplitudes reach a limit value at a reduced velocity higher than 5.7. At the instability onset, the vibration frequency was equal to the natural frequency of the system. Its value was roughly doubled at $U \approx 5.7$, and it appears that it maintains this trend of increase for reduced velocities greater than 5.7. This means that, as the flow velocity was increased, the wake-induced forces caused the oscillation to become progressively faster.

With an increase in the separation to 1.5 diameters (test T2), the value of reduced velocity for galloping onset increased slightly to $U_0 \approx 0.7$. Figure 9(*b*) shows that the vibration amplitude sharply increases with increasing flow speed until a peak is reached at a reduced velocity of about 1.2. This value is greater than the corresponding vortex-resonance speed. Further increases in the flow velocity cause the oscillation amplitude to decrease rapidly until a reduced velocity of $U \approx 1.8$, beyond which the trend reverses, with the vibration amplitude having a slow increase as the flow velocity is increased. Again it appears that the oscillation amplitudes attain a limit value at a reduced velocity greater than 5.7. This excitation is recognized as a combined vortex resonance and galloping; the galloping being suppressed by the influence of the nearby vortex lock-in. The vortex-resonance portion of the instability

Run (1)	Longitudinal-spacing ratio x_0 (2)	Lateral-spacing ratio y_0 (3)	Natural circular frequency ω_n (rad/s) (4)	Vibratory Reynolds number $\gamma = \frac{\omega_n D^2}{\nu}$ ($\nu = 10^{-6}$ m^2/s) (5)	Added-mass coefficient C_M (6)	Reduced damping $\beta = \frac{c}{2m\omega_n}$ (7)	Mass parameter $n = \frac{\rho D^2 L}{2m}$ ($\rho \approx 10^3$ kg/m^3) (8)	Vortex-resonance speed $U_r = \frac{1}{2\pi S_2}$ (9)	Stability parameter $k_s = \frac{2\pi\beta}{n}$ (10)	Reynolds-number range $Re = \frac{VD}{\nu}$ ($\nu = 10^{-6}$ m^2/s) (11)
T1a†	1.09	0.00	4.11	1052	1.68	0.0129	0.0756	0.76	1.072	600–6000
T1b‡	1.09	0.00	4.54	291	2.13	0.0307	0.0378	0.76	5.103	200–1900
T1c†,‖	1.09	0.00	4.10	1050	1.68	0.0651	0.0751	0.76	5.447	800–5800
T1d†	1.09	0.00	4.10	1050	1.68	0.1105	0.0751	0.76	9.245	800–5500
T1e†	1.09	0.00	4.10	1050	1.69	0.1587	0.0751	0.76	13.278	800–5750
T2†	1.50	0.00	4.11	1052	1.69	0.0129	0.0756	0.97	1.072	800–5800
T3†	2.00	0.00	4.11	1052	1.69	0.0129	0.0756	1.05	1.072	800–5800
T4†	2.50	0.00	4.11	1052	1.67	0.0129	0.0756	1.13	1.072	650–5800
T5†	3.00	0.00	4.11	1052	1.68	0.0129	0.0756	1.15	1.072	750–5800
T6†	4.00	0.00	4.11	1052	1.67	0.0129	0.0756	0.97	1.072	750–1800
T7†	5.00	0.00	4.11	1052	1.67	0.0129	0.0756	0.89	1.072	700–2000
P1†	1.09	0.50	4.11	1052	1.67	0.0124	0.0756	1.37	1.031	750–6000
P2†	1.50	0.50	4.11	1052	1.67	0.0124	0.0756	1.30	1.031	750–6000
P3†	2.00	0.50	4.11	1052	1.69	0.0124	0.0756	1.23	1.031	700–6000
P4†	2.50	0.50	4.11	1052	1.69	0.0124	0.0756	1.20	1.031	650–6000
P5†	3.00	0.50	4.11	1052	1.68	0.0124	0.0756	1.09	1.031	650–2000
P6†	4.00	0.50	4.11	1052	1.68	0.0124	0.0756	0.98	1.031	600–2000
P7†	5.00	0.50	4.11	1052	1.68	0.0124	0.0756	0.90	1.031	600–2000

Q1†	1.09	1.00	4.11	1052	1.70	0.0126	0.0755	1.33	1.049	1050–5900
Q2†	1.50	1.00	4.11	1052	1.70	0.0126	0.0755	1.20	1.049	1025–5700
Q3†	2.00	1.00	4.11	1052	1.70	0.0126	0.0755	1.21	1.049	950–5700
Q4†	2.50	1.00	4.11	1052	1.68	0.0126	0.0756	1.11	1.047	900–1900
Q5†	3.00	1.00	4.11	1052	1.69	0.0126	0.0756	1.10	1.047	900–1900
Q6†	4.00	1.00	4.11	1052	1.69	0.0126	0.0756	0.93	1.047	900–1900
Q7†	5.00	1.00	4.11	1052	1.69	0.0126	0.0756	0.89	1.047	600–1900
R1†	1.09	2.00	4.11	1052	1.67	0.0129	0.0756	0.79	1.072	700–1900
R2†	1.50	2.00	4.11	1052	1.67	0.0129	0.0756	0.81	1.072	700–2000
R3†	2.00	2.00	4.11	1052	1.67	0.0129	0.0756	0.82	1.072	600–1800
R4†	3.00	2.00	4.11	1052	1.67	0.0129	0.0756	0.81	1.072	600–1800
R5†	4.00	2.00	4.11	1052	1.67	0.0129	0.0756	0.78	1.072	600–1800
R6†	5.00	2.00	4.11	1052	1.67	0.0129	0.0756	0.81	1.072	600–1700
S1†	1.09	3.00	4.11	1052	1.67	0.0129	0.0756	0.74	1.072	670–1650
S2†	1.50	3.00	4.11	1052	1.67	0.0129	0.0756	0.74	1.072	600–1700
S3†	2.00	3.00	4.11	1052	1.67	0.0129	0.0756	0.74	1.072	600–1700
S4†	3.00	3.00	4.11	1052	1.67	0.0129	0.0756	0.76	1.072	600–1700
S5†	4.00	3.00	4.11	1052	1.67	0.0129	0.0756	0.73	1.072	600–1700
S6†	5.00	3.00	4.11	1052	1.67	0.0129	0.0756	0.73	1.072	600–1700

† Cylinder made of PVC; cylinder diameter $D = 16$ mm; cylinder length $L = 298$ mm; cylinder aspect ratio $L/D = 18.63$; initial-displacement ratio $\eta = Y_0/D = 3.13$.

‡ Cylinder made of dural; cylinder diameter $D = 8$ mm; cylinder length $L = 298$ mm; cylinder aspect ratio $L/D = 37.25$; initial-displacement ratio $\eta = Y_0/D = 6.26$.

‖ Wake observations behind the vibrating cylinder.

TABLE 1. Characteristics of the dynamic tests

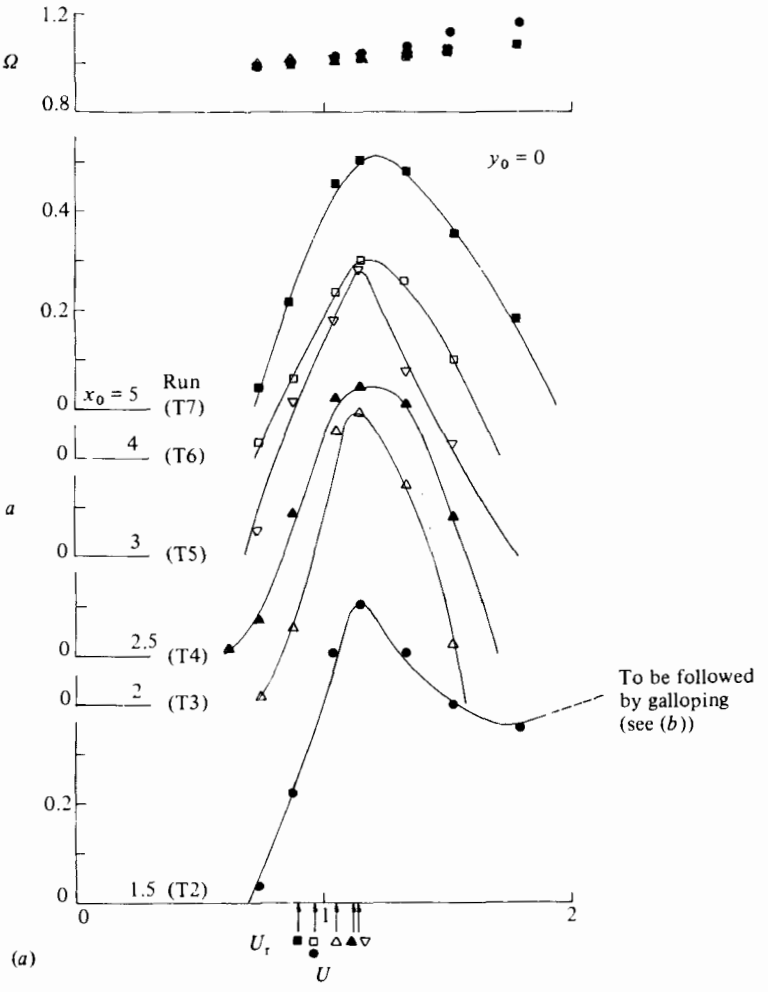

FIGURE 9(a). For caption see facing page.

can be seen in a magnified form in figure 9(a). This figure denotes that throughout a major part of lock-in range the vibration frequency only slightly deviates from the system's natural frequency. However, as can be seen in figure 9(b), the oscillation-frequency data at 1.5 diameters position generally have the same pattern as those at $x_0 = 1.09$. They collapse onto one another for reduced velocities less than 2.6.

With further increases in the spacing to 2, 2.5 and 3 diameters, corresponding to runs T3, T4 and T5 respectively, the cylinder underwent a separated vortex resonance and galloping instability. At these positions the vortex-induced excitation ended in a very small range $1.6 \lesssim U \lesssim 1.8$. At two diameters separation, the galloping part of the instability began at a reduced velocity of about 2.65, which is considerably higher than the corresponding value at $x_0 = 1.09$, while at positions $x_0 = 2.5$ and 3 it started at a higher value of $U_0 \approx 3.2$. The galloping behaviour at 2, 2.5 and 3 diameters spacings, both in amplitude and frequency domains, is very similar to that at $x_0 = 1.09$. It is interesting to note that at these stations the peak lock-in amplitude is approximately equal to the corresponding limit galloping amplitude, but is almost half of that at $x_0 = 1.09$ (test T1a). From the above observations, it may be inferred that in tandem arrangement, with increasing gap, the continually increasing galloping-

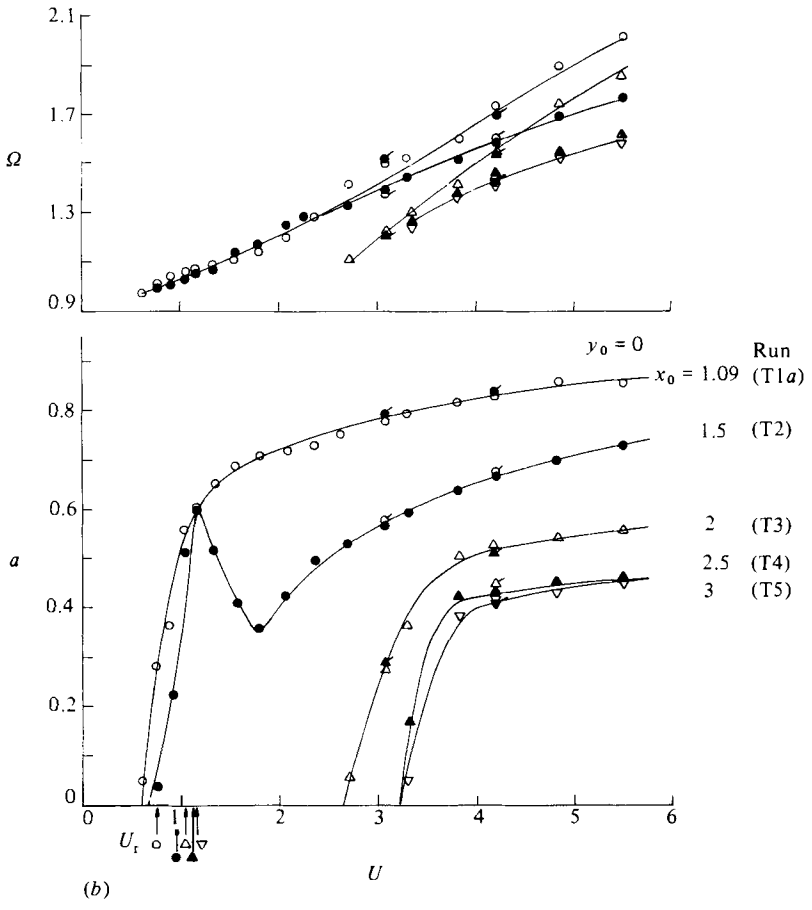

FIGURE 9. Variation of the reduced amplitude and the oscillation-frequency ratio versus the reduced velocity in tandem arrangement: ○, ◐, $x_0 = 1.09$; ●, ◑, 1.5; △, ◭, 2.0; ▲, ◬, 2.5; ▽, ▼, 3.0 (the first symbol represents the 6.5% turbulence intensity while the second one denotes the 11.9% turbulence level); □, 4.0; ■, 5.0 (6.5% turbulence intensity).

amplitude profile tends to break into a separated vortex resonance and galloping instability; the galloping amplitudes generally decrease; and the vibration generally becomes slower (the oscillation frequency decreases). All of these are only true if the gap remains sufficiently small. As figure 9 indicates, at larger separations of 4 and 5 diameters the cylinder exhibited only a vortex lock-in. A close examination of all vortex-resonance data in tandem arrangement in figure 9(*a*) shows that the peak lock-in amplitude occurred at a reduced velocity of about 1.2. Furthermore it indicates that the vibration-frequency data of the runs other than T2 fall onto one another, with the oscillation frequency increasing slightly, around the natural frequency of the system, as the flow speed is increased. In test T2, where a combined vortex resonance and galloping occurred, away from lock-in, the vibration frequency showed considerable increase with increasing flow velocity.

In dynamic test observations of staggered arrangements, depending on the relative position of the cylinder pair, either a vortex lock-in or a separated vortex resonance and galloping instability was observed. In both cases, in the lock-in range, the trend of the variation of the relative oscillation frequency versus the reduced velocity is almost the same as that observed in tandem arrangement at large spacings. The

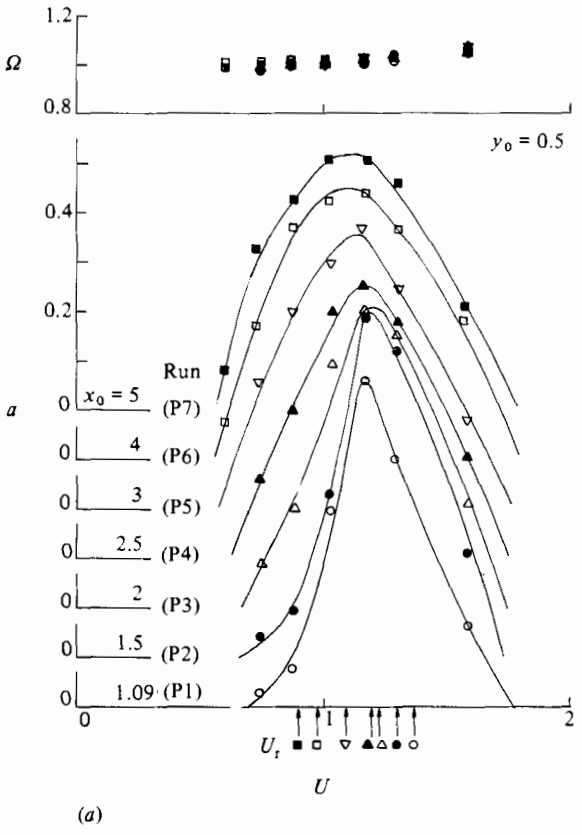

(a)

FIGURE 10(a). For caption see facing page.

results with lateral spacing of 0.5 diameters are shown in figure 10. For the sake of clarity, the galloping and vortex-resonance data are plotted separately in figures 10(*b*) and (*a*) respectively. The cylinder mean position indicated no appreciable variation with increased free-stream flow speed. The vibrations began in the reduced-velocity range $0.55 \lesssim U \lesssim 0.7$, which is very close to the corresponding one of tandem arrangement.

Figure 10 shows that in runs P1, P2, P3 and P4, having small longitudinal separations of 1.09, 1.5, 2 and 2.5 respectively, the cylinder exhibited a separated vortex resonance and galloping. It can be seen again that the galloping amplitudes generally decrease on increasing the streamwise gap, and the limit galloping amplitude is roughly equal to the corresponding peak lock-in amplitude. At larger spacings of 3, 4 and 5 diameters, associated with tests P5, P6 and P7 respectively, only a vortex-induced oscillation occurred. The reduced-amplitude profiles in figure 10(*a*) clearly indicates that, as the longitudinal gap is increased, the vibrations begin at a smaller flow speed, the peak resonance amplitude generally decreases, both the reduced velocity at peak lock-in amplitude and the vortex-resonance speed decrease, and the vortex lock-in shape generally becomes broader. The vortex-excited oscillations all end at a reduced velocity of about 1.75.

A comparison of figures 9(*b*) and 10(*b*) reveals that, in the amplitude domain, the galloping profiles of staggered arrangement at 1.09, 1.5, 2 and 2.5 diameters streamwise position are similar to those of tandem arrangement, which have larger separations. For a given longitudinal gap, the galloping instability in staggered

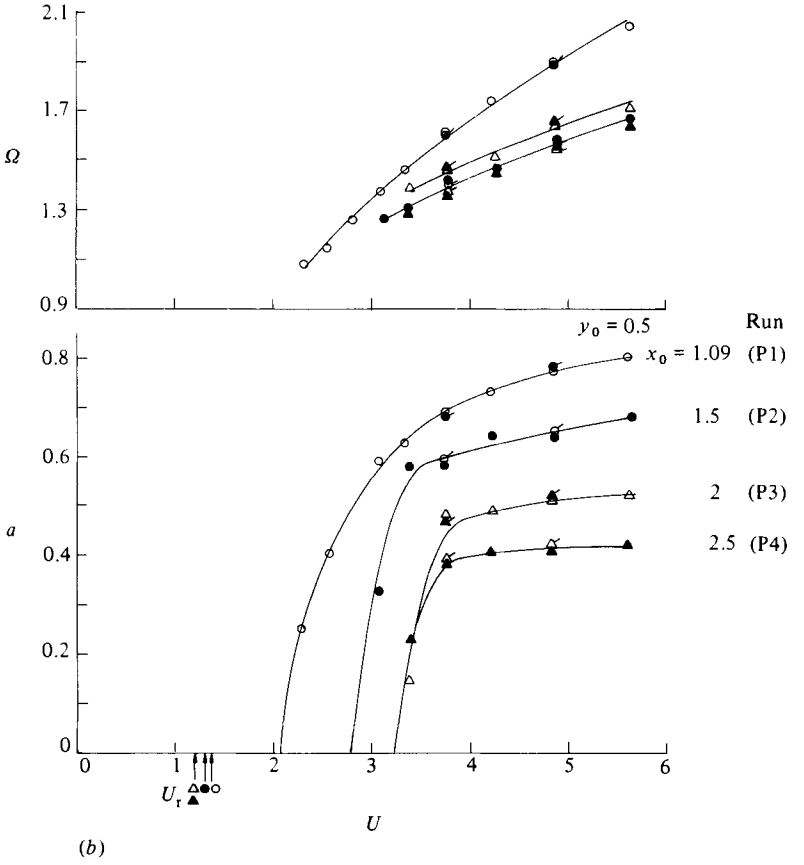

FIGURE 10. Variation of the reduced amplitude and the oscillation frequency ratio versus the reduced velocity in staggered arrangement. Symbols as figure 9.

arrangement generally begins at a reduced velocity which is higher than the corresponding value of tandem arrangement, and also reaches a limit value quicker. For example, at $x_0 = 2$ in staggered arrangement (run P3), the galloping excitation started at reduced velocity of about $U_0 = 3.2$, and it appears that it attained a limit vibration amplitude at about $U \approx 6$. For the same streamwise spacing in tandem arrangement (test T3), the galloping vibration began at $U_0 \approx 2.65$, and as figure 9(*b*) denotes, at $U = 6$ the oscillation amplitude still shows an increase with increasing flow speed. However, in the frequency domain, the galloping profiles in staggered arrangement have the same trend as the corresponding ones in tandem arrangement. It is interesting to note that the vibration-frequency profiles at separations $x_0 = 1.09$ and 2.5 in staggered arrangement are almost identical with the corresponding ones in tandem arrangement. One important conclusion from the dynamic observations described so far is that the behaviour of wake-induced galloping, in both the amplitude and frequency domains, is entirely different from that of galloping of isolated non-circular cylinders, in which the oscillation frequency remains at a constant value, and, at sufficiently high values of reduced velocity, the amplitude varies almost linearly in relation to flow speed (Blevins 1979).

The measured results with one diameter transverse spacing are drawn in figure 11, with vortex-resonance and galloping data being plotted separately. At small

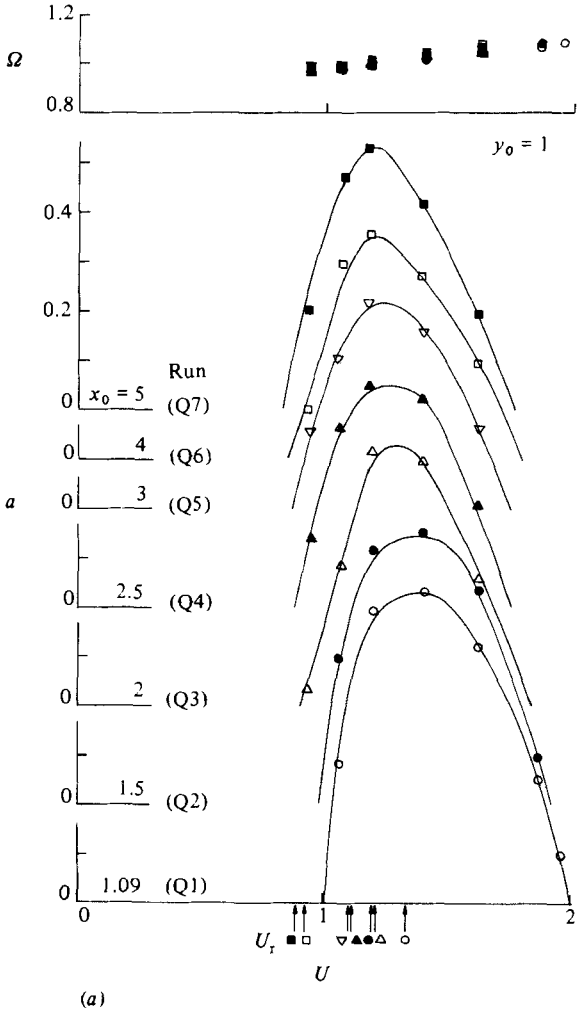

FIGURE 11 (*a*). For caption see facing page.

longitudinal separations of 1.09, 1.5 and 2 diameters, represented by runs Q1, Q2 and Q3 respectively, the cylinder underwent a separated vortex resonance and galloping instability, while at larger spacings it exhibited only a vortex lock-in. The vortex-resonance profiles are similar amongst themselves. The vibration began in a narrow reduced-velocity range $0.75 \lesssim U \lesssim 1$. This range is higher than the corresponding ones in tandem and staggered arrangement with $y_0 = 0.5$ (see figures 9*a*, 10*a*). As figure 11 (*a*) clearly shows, as the streamwise gap is increased, the vortex-excited oscillation begins at a smaller flow speed, the peak lock-in amplitude, the corresponding reduced velocity and the vortex-resonance speed all decrease, and the vortex lock-in ends at a smaller flow velocity. Again at each value of the cylinder separation, some difference can be seen between the reduced velocity at peak resonance amplitude, and the corresponding vortex-resonance speed.

An interesting point in the galloping profiles with $y_0 = 1$ (figure 11*b*) is that the variation of the vibration frequency ratio against the reduced velocity at positions

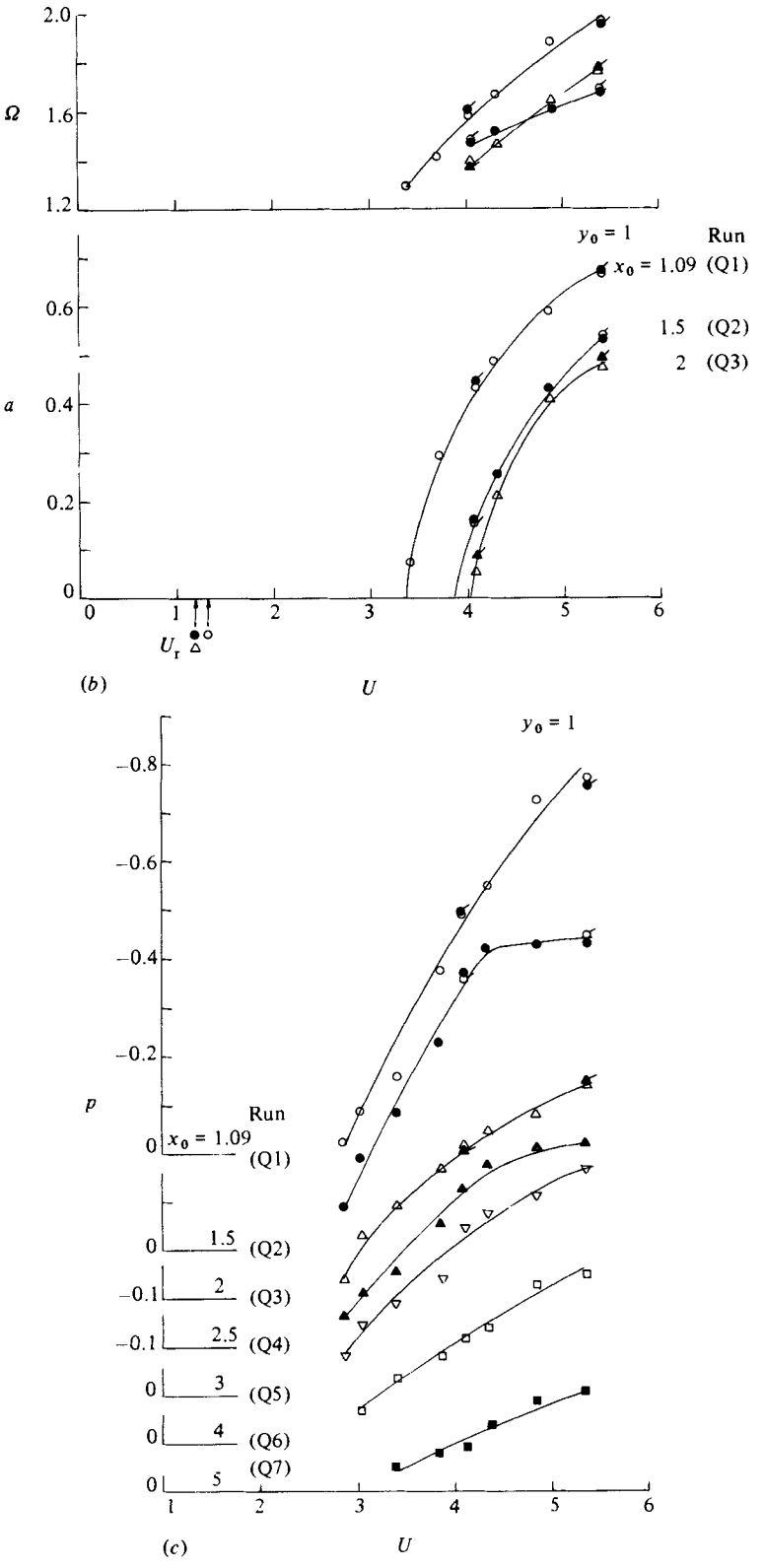

FIGURE 11. Variation of the reduced amplitude, the oscillation-frequency ratio and the cylinder mean position versus the reduced velocity in staggered arrangement. Symbols as figure 9.

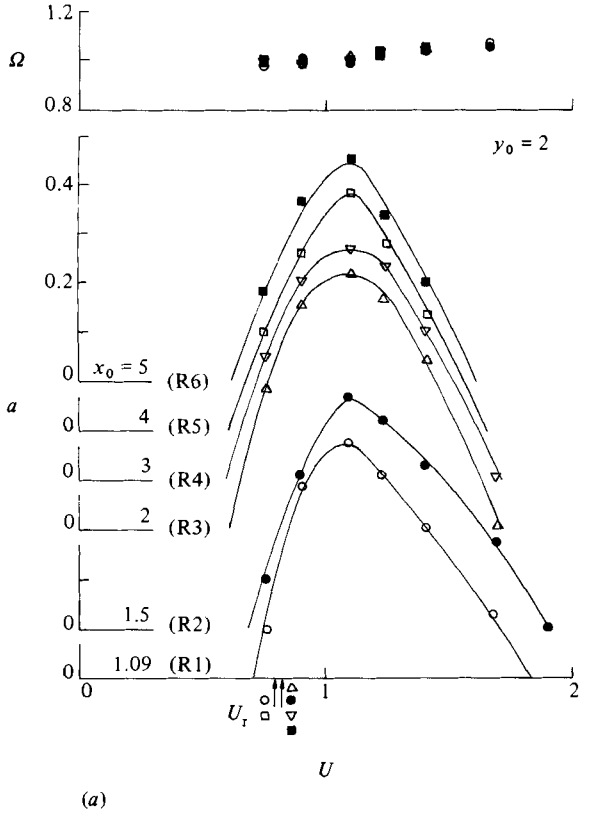

(a)

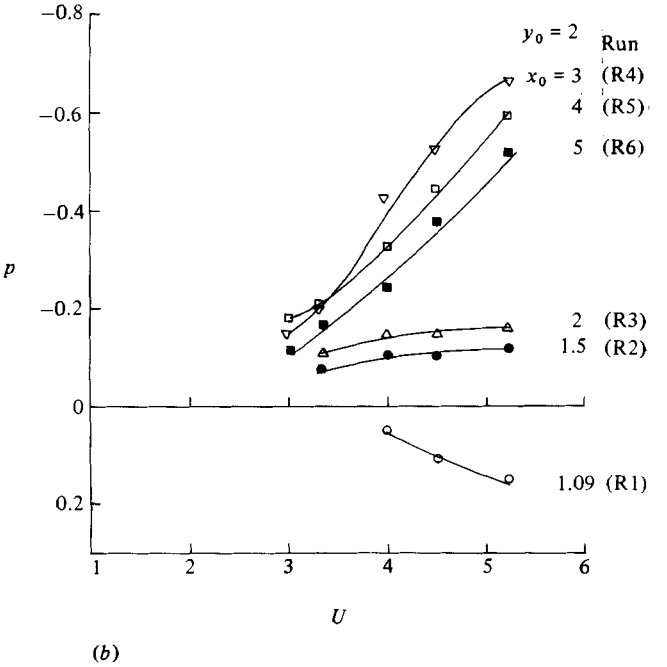

(b)

FIGURE 12. Variation of the reduced amplitude, the oscillation-frequency ratio, and the cylinder mean position versus the reduced velocity in staggered arrangement. Symbols as figure 9.

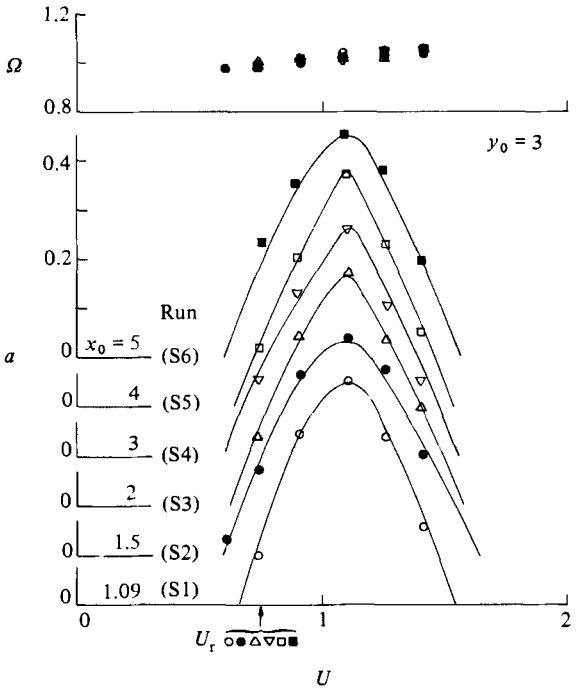

FIGURE 13. Variation of the reduced amplitude and the oscillation-frequency ratio versus the reduced velocity in staggered arrangement. Symbols as figure 9.

$x_0 = 1.09$ and 1.5 is almost identical with the corresponding ones of $y_0 = 0.5$, which itself is nearly identical with the corresponding ones of tandem arrangement. Another interesting point is the variation of the cylinder mean position in relation to flow speed just before the onset of galloping instability (when the cylinder was almost stationary), and during galloping oscillations. As figure 11 (*c*) shows, the direction of displacement of the cylinder mean position is opposite to that of transverse separation y_0. This means that, in staggered arrangement with one diameter lateral spacing, the wake-excited galloping forces tended to make the cylinder pair aligned with one another. At the smallest gap ($x_0 = 1.09$), the cylinder mean position varied sharply with changing flow velocity, and it appears that at the reduced velocity of about 6 the mean position of galloping cylinder became almost aligned with that of the upstream body. Notice that at separations $x_0 = 2.5$, 3, 4 and 5, associated with experiments Q4, Q5, Q6 and Q7 respectively, where only a vortex resonance occurred, at high reduced velocities outside the lock-in range, while the cylinder remained stationary, its mean position varied with flow speed. A comparison of all profiles in figure 11 (*c*) reveals that, with an increase in the longitudinal gap, the rate of increase of the cylinder mean position in relation to flow velocity generally decreases, and a higher flow speed is needed for this phenomenon to begin.

The galloping vibration data in tandem and staggered arrangements, either in the form of a galloping instability alone or a combined or separated vortex resonance and galloping excitations, have demonstrated a number of important features. First, the galloping amplitudes and frequencies remain essentially unaffected by a limited increase in free-stream turbulence intensity. Secondly, the vibrations always build up from an equilibrium position (cylinder position in still fluid). These characteristics of wake-induced galloping are in contrast to those of galloping of isolated sharp-edged

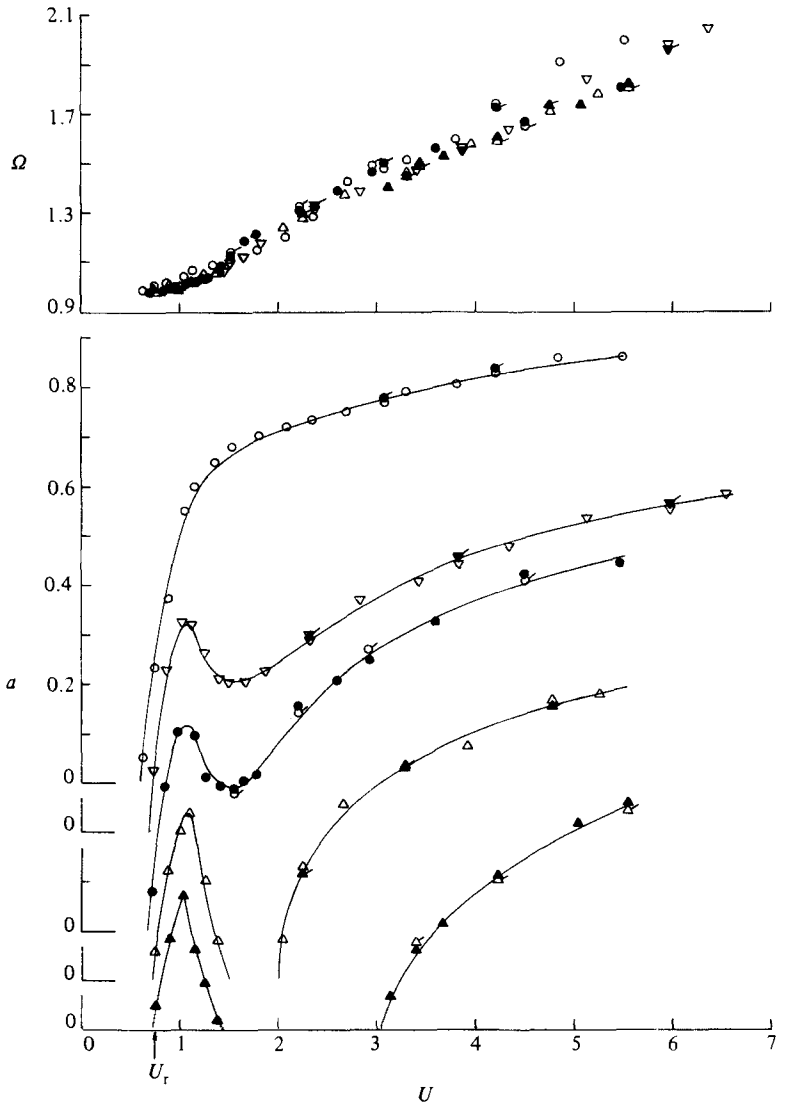

FIGURE 14. Variation of the reduced amplitude and the oscillation-frequency ratio versus the reduced velocity in tandem arrangement at different stability-parameter levels: ○, ◐, run T1*a*; ▽, ▼, T1*b*; ●, ◌, T1*c*; △, ◭, T1*d*; ▲, ◬, T1*e* (the first symbol represents the 6.5% turbulence intensity while the second one denotes the 11.9% turbulence level).

bodies, in which, depending on the cross-sectional geometry, the free-stream turbulence can have profound effects on the cylinder instability, and some initial displacement (triggering amplitude) may be required to excite the cylinder to gallop (Blevins 1979). Thirdly, the above data indicate that for a fixed streamwise gap, on increasing the transverse separation, a higher free-stream flow velocity is required in order to excite the cylinder to gallop. This means that the effect of increasing the flow speed is to extend the area of instability further downstream.

Figures 12 and 13 show the results associated with two and three diameters lateral spacing respectively. Only a vortex-excited resonance can be seen in these figures. The profiles with $y_0 = 3$ are very similar to one another. At the cylinder separations shown in these two figures, the vibrations began in the reduced velocity range

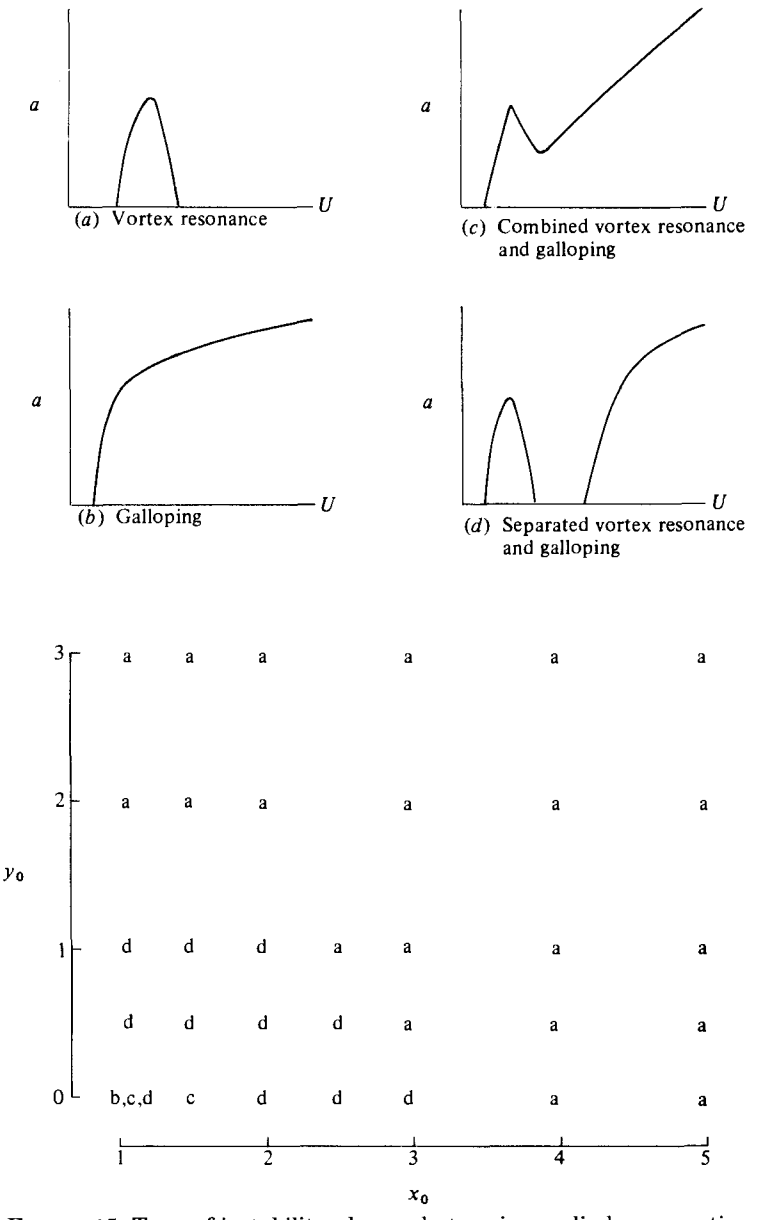

FIGURE 15. Type of instability observed at various cylinder separations.

$0.6 < U < 0.7$, which is lower than the corresponding range of $y_0 = 1$, but is near to those of $y_0 = 0$ and 0.5 (see figures 9*a*, 10*a*). In both figures 12 and 13 the resonance amplitude peaks at a reduced velocity of about 1.1. At two diameters transverse separation, at reduced velocities above the lock-in range where the cylinder was almost stationary, the body mean position varied with an increase in the flow speed. However, no such variation occurred at three diameters lateral spacing.

It is known that galloping amplitudes of isolated bluff bodies are sensitive to cylinder aspect ratio. The effects of change in the aspect ratio of the cylinder pair on the behaviour of wake-induced galloping can be found by comparing the dynamic test results of runs T1*b* and T1*c*, as indicated in figure 14. The two experiments have

significantly different aspect ratios but possess the same separation, and were designed to have roughly the same value of stability parameter. This figure denotes that an increase in the aspect ratio from $L/D = 18.63$ to 37.25 caused some differences in the oscillation amplitude, though the vibration frequencies remained essentially unaffected. These observations clearly demonstrate that wake-induced galloping amplitudes are also sensitive to cylinder aspect ratio.

The increase in structural damping, apart from generally reducing the oscillation amplitudes, can drastically affect the cross-flow response of isolated bluff bodies (Wawzonek & Parkinson 1979; Bokaian & Geoola 1984*a*). The effects of change in structural damping on the behaviour of wake-induced galloping can be found by comparing the results of tests T1*a*, T1*c*, T1*d* and T1*e*, as indicated in figure 14. In these experiments the cylinder pair was in tandem arrangement, and had a separation of 1.09 diameters. This spacing was deliberately chosen because the oscillation amplitudes were the greatest at that point (see figure 9*b*). The above runs have significantly different stability-parameter values. The effects of increasing the structural damping on the wake-excited instability can be seen to be quite striking. It generally causes the vibration to begin at a slightly higher flow speed. An increase in the value of k_s from 1.072 (run T1*a*) to 5.447 (run T1*c*) changes the continually increasing galloping amplitude profile into a combined vortex resonance and galloping excitation. With further increases in the value of stability parameter to 9.245 (run T1*d*) and 13.278 (run T1*e*), a separated vortex resonance and galloping instability appear in the reduced amplitude profiles.

An interesting point is that in tests other than T1*a* the lock-in amplitude peaks at about the same reduced velocity, and the vortex resonance ends at the reduced velocity of approximately $U = 1.5$. A further interesting point is that in the reduced-amplitude profile of run T1*a* the slope of the curve changes around the abovementioned velocity. From these one may suspect that in these experiments the mechanism of instability somehow changed at $U \approx 1.5$. As is to be expected, as the structural damping is increased, the oscillation amplitudes decrease, and a higher free-stream flow speed is needed for galloping to commence. The effects of changing the stability parameter on the variation of relative vibration frequency in relation to reduced velocity appears to be rather inappreciable. These characteristics of wake-induced galloping are similar to those of galloping of single sharp-edged bodies. The above observations show once again that a limited increase in the free-stream turbulence intensity has no bearing on the behaviour of wake-excited galloping.

4.4. *Wake fluctuations behind the galloping cylinder*

In test T1*c* the velocity fluctuations in the wake of the vibrating body were measured at various flow speeds. This experiment was deliberately chosen since the cylinder exhibited a combined vortex-resonance and galloping instability (see figure 14). The aim was to examine the vortex-shedding frequency during both the vortex lock-in and galloping parts of the excitation. Table 1 indicates that in this run the natural circular frequency of the system was $\omega_n = 4.1$ rad/s. As can be seen in the above figure, the oscillation began at a reduced velocity of about $U = 0.7$, and the lock-in region spanned the range $0.7 \lesssim U \lesssim 1.5$. At the instability onset the vibration circular frequency ω_c was slightly less than ω_n. The value of ω_c indicated a slow increase with increasing flow velocity, and reached the value of ω_n at a reduced velocity equal to the vortex-resonance speed U_r. At the end of the vortex-excited resonance the oscillation frequency was only slightly higher than the system's natural frequency.

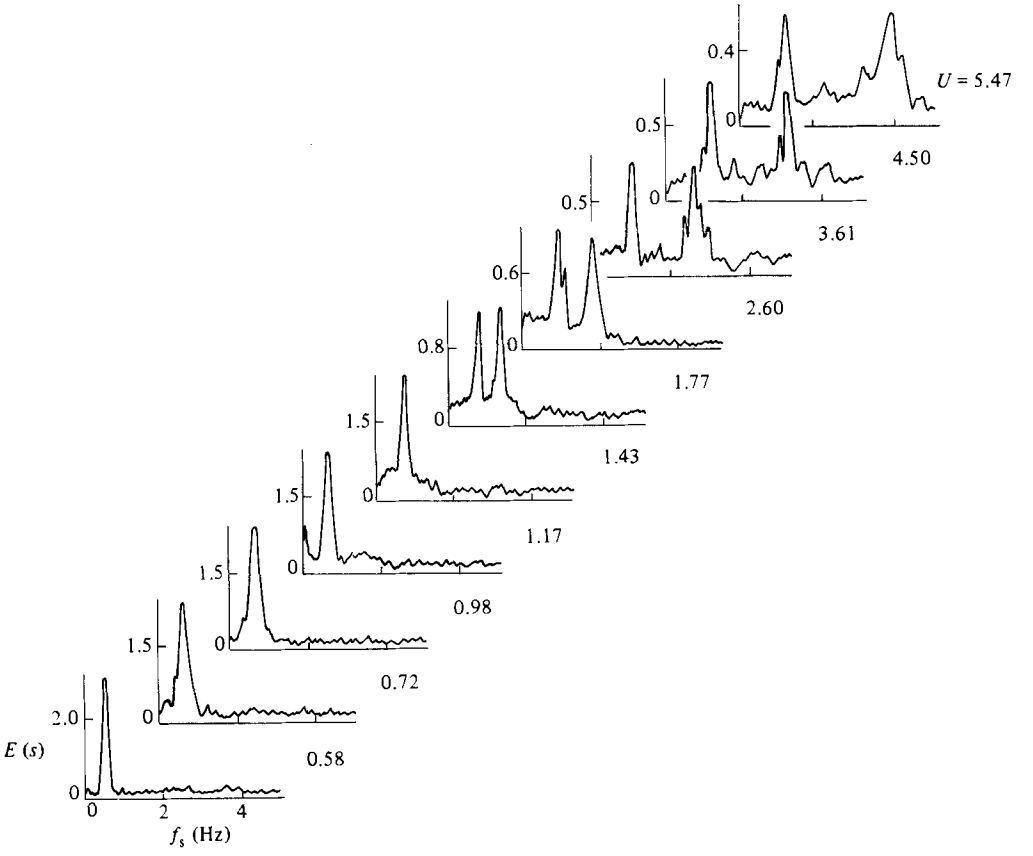

FIGURE 16. Normalized spectral-density plots of wake fluctuations behind the vibrating cylinder in test T1*c* ($(\overline{v^2})^{\frac{1}{2}}/V = 6.5\,\%$).

The hot-film probe was positioned in the centreplane of the flume on one side of the downstream body's wake, and the fluctuating velocity at a given flow speed was recorded. Figure 16 presents typical examples of the power spectra of the vibrating body's wake at various flow velocities, with E and f denoting the normalized spectral density and the shedding frequency respectively. Indicated on the right-hand side of each figure is the corresponding reduced velocity. Figure 17 summarizes the variation of the dimensionless vortex-shedding frequency ω_s/ω_n, where ω_s is the circular vortex-shedding frequency as estimated from the peak in the power spectrum, in relation to reduced velocity.

As can be seen in figure 16, the power spectra at reduced velocities of $U = 0.58$, 0.72, 0.98, 1.17 and 1.43, which belong to the vortex-lock-in range, all indicate a single clear and pronounced peak at a predominant frequency. This means that the wake was fluctuating in a fairly sinusoidal manner, and hence the presence of a strong vortex-shedding process. Figure 17 clearly denotes that at oscillation onset the vortex-shedding frequency was slightly less than the system's natural frequency ω_n. On increasing the flow velocity, the value of ω_s also increased and became equal to that of ω_n at a reduced velocity equal to the vortex-resonance speed U_r. At the end of the vortex-excited resonance the shedding frequency was only slightly higher than the natural frequency of the system. The variation of the dimensionless vortex-shedding frequency versus reduced velocity U is identical with the corresponding one of ω_c/ω_n with U. Visualization of flow patterns by injecting potassium permanganate

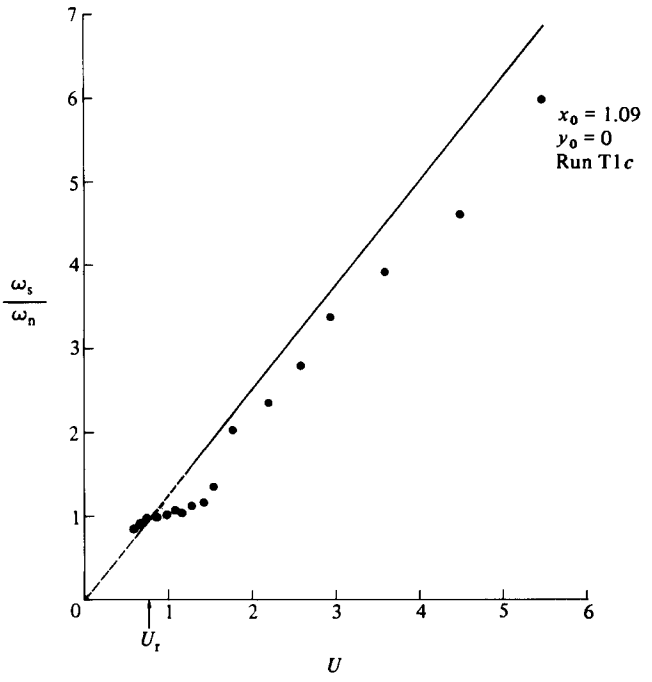

FIGURE 17. Variation of the dimensionless vortex-shedding frequency behind the vibrating cylinder versus the reduced velocity in test T1 c ($(\overline{v^2})^{\frac{1}{2}}/V = 6.5\%$).

into the vibrating cylinder's wake indicated that during vortex lock-in a pair of vortices was regularly formed during one cycle of oscillation. From these findings it may be inferred that, during the vortex-resonance part of the instability, the shedding frequency locked to the vibration frequency. This is an evidence that in the range $0.75 \lesssim U \lesssim 1.5$ the excitation was a genuine vortex resonance.

As described earlier, in experiment T1c, the galloping frequency continually increased as the flow speed was increased (see figure 14). In figure 16 the power spectra at reduced velocities of $U = 1.77, 2.60, 3.61, 4.50$ and 5.47, which are associated with the galloping range, all depict two peaks. A marked feature of these spectra is that, on increasing the flow velocity, the spectra generally become broader, with the peaks becoming less distinct than those of vortex-resonance excitation. The frequency of the first peak steadily increases as the reduced velocity U is increased, and its variation with U is almost identical with that of relative oscillation frequency ω_c with U (see figure 14). From this one may conclude that the first peak represents the vibration frequency while the second one denotes the shedding frequency. The power spectra clearly demonstrate that the shedding frequency during galloping oscillations continually increased with increasing flow velocity. A comparison of figures 14 and 17 reveals that in the galloping range the rate of increase of the dimensionless vortex-shedding frequency ω_s/ω_n versus reduced velocity U is higher than the corresponding one of the vibration-frequency ratio ω_c/ω_n against U. Wake observations behind the oscillating body confirmed that in one vibration cycle more than one pair of vortices was regularly shed. From these findings it may be deduced that in wake-induced galloping the vortex-shedding frequency is higher than the vibration frequency. This can also be inferred from the power-spectra plots of figure 16.

It is known that the Strouhal number of vortex shedding behind a single galloping

cylinder behaves as if the body was stationary; that is, the shedding frequency varies linearly with flow velocity. An attempt was made to examine whether the wake-excited galloping has this characteristic. In test T1*c* the cylinder pair was in tandem arrangement with a separation of 1.09 diameters. In this arrangement and at this spacing the Strouhal number of vortex shedding behind the stationary downstream cylinder (see figure 4) is $S_2 = f_s V/D = 0.20$. This relationship can be written in the form

$$\frac{\omega_s}{\omega_n} = 2\pi S_2 U = 1.26U. \tag{1}$$

The straight line in figure 17, which generally lies above the experimental data, depicts the above equation. As this figure shows, in the reduced-velocity range $1.7 \lesssim U \lesssim 3$ where the oscillation amplitudes were rather small (less than 0.5 diameters), the deviation of the data points from the straight line is rather small. From these observations it may generally be inferred that during galloping motion the vortex-shedding frequency behaved roughly as if the cylinder was stationary. This characteristic of wake-induced galloping, though valid only for small vibration amplitudes, is identical with that of galloping of isolated non-circular cylinders.

5. Review and conclusions

Various phenomena associated with flow around a stationary or oscillating circular cylinder in the wake generated by a fixed identical upstream body were investigated. Static-force data displayed a number of interesting features. The variation of lift and drag coefficients was observed to be respectively antisymmetrical and symmetrical with respect to the wake centreline; the minimum drag force being on this line. Throughout most of the wake the forces on the rear body were found to have a lateral component towards the wake centreline, and a streamwise component. It was observed that the drag coefficient is a continuous function of the cylinder separation. The transverse extent of the force field indicated an increase with increasing longitudinal spacing. Static data quite clearly indicated that turbulence is an important parameter when considering the characteristics of drag forces. Its effects were observed to be quite noticeable for transverse separations greater than two diameters. It was generally inferred that the three independent parameters of Reynolds number, turbulence characteristics and cylinder aspect ratio, collectively or individually, are significant parameters in the static tests.

In dynamic tests, performed over the reduced-velocity range 0–6, the behaviour of the vibrating cylinder showed differing characteristics depending on structural damping and cylinder separation. The galloping motion was always found to build up from an equilibrium position, with the galloping extent increasing further downstream as the flow velocity is increased. It was observed that, whereas the characteristics of wake-induced instability are essentially unaffected by a limited change in turbulence intensity, the galloping amplitudes are rather sensitive to cylinder aspect ratio. The results clearly showed that the galloping frequency can have substantial variation with flow speed. Moreover, they indicated that an increase in the stability parameter, apart from generally reducing the vibration amplitudes, can drastically change the nature of the cylinder response, particularly in the amplitude domain.

Wake observations behind the vibrating body showed that in vortex-excited lock-in the frequency of vortex-shedding locked to oscillation frequency, but during small-amplitude galloping motion the shedding frequency behaved as if the cylinder was

stationary. Whilst some characteristics of wake-excited galloping were found to be similar to those of galloping of sharp-edged bodies, others were observed to be fundamentally different. Still-water tests indicated that the added mass of the vibrating cylinder was independent of the vibration amplitude, and was very little affected by its proximity to a fixed identical body.

The authors wish to acknowledge the support of London Centre for Marine Technology for the research programme that resulted in this paper. Special thanks are due to Professor J. M. T. Thompson for his support and encouragement. The experimental part of this work was conducted in the hydraulics laboratory of Imperial College, London. The authors are grateful to Mr M. J. Kenn for his generous assistance.

REFERENCES

Blevins, R. D. 1977 *Flow-Induced Vibration.* Van Nostrand Reinhold.

Bokaian, A. & Geoola, F. 1984*a* Hydroelastic instabilities of square cylinders. *J. Sound Vib.* **92**, 117–141.

Bokaian, A. & Geoola, F. 1984*b* Vortex-shedding from two interfering circular cylinders. *Tech. Note, J. Engng Mech. Div., ASCE* **110**, 623–628.

Chen, S. S., Wambsganss, M. W. & Jendrzejczyk, J. A. 1976 Added mass and damping of a vibrating rod in confined viscous fluids. *Trans. ASME* E: *J. Appl. Mech.* **98**, 325–329.

Cooper, K. R. 1974 Wind tunnel measurements of the steady aerodynamic forces on a smooth circular cylinder immersed in the wake of an identical cylinder. *Natl Aero. Estab., Canada,* LTR-LA-119.

Cooper, K. R. & Wardlaw, R. L. 1971 Aeroelastic instabilities in wake. In *Proc. Intl Symp. on Wind Effects on Buildings and Structures, Tokyo; Paper* IV. 1, pp. 647–655.

Hori, E. 1959 Experiments on flow around a pair of parallel circular cylinders. In *Proc. 9th Japan Natl Congr. Appl. Mech., Tokyo,* pp. 231–234.

Jendrzejczyk, J. A., Chen, S. S. & Wambsganss, M. W. 1979 Dynamic responses of a pair of circular tubes subjected to liquid cross flow. *J. Sound Vib.* **67**, 263–273.

King, R. & Johns, D. J. 1976 Wake interaction experiments with two flexible circular cylinders in flowing water. *J. Sound Vib.* **45**, 259–283.

Kiya, M., Suzuki, Y., Arie, M. & Hagino, M. 1982 A contribution to the free-stream turbulence effect on the flow past a circular cylinder. *J. Fluid Mech.* **115**, 151–164.

Kostic, Z. G. & Oka, S. N. 1972 Fluid flow and heat transfer with two cylinders in cross flow. *Intl J. Heat Mass Transfer* **15**, 279–299.

Price, S. J. 1975 Wake-induced flutter of power transmission conductors. *J. Sound Vib.* **38**, 125–147.

Price, S. J. 1976 The origin and nature of the lift force on the leeward of two bluff bodies. *Aero. Q.* **26**, 154–168.

Roberts, B. W. 1966 Low frequency aeroelastic vibrations in a cascade of circular cylinders. *Mech. Engng Sci. Monograph* no. 4.

Ruscheweyh, H. P. 1983 Aeroelastic interference effects between slender structures. In *Proc. 6th Intl Conf. on Wind Engng, Gold Coast, Australia & Auckland, N.Z.*

Simpson, A. 1971 On the flutter of a smooth circular cylinder in a wake. *Aero. Q.* **22**, 25–41.

Tanida, Y., Okajima, A. & Watanabe, Y. 1973 Stability of a circular cylinder oscillating in uniform flow or in a wake. *J. Fluid Mech.* **61**, 769–784.

Vickery, B. J. & Watkins, R. D. 1964 Flow-induced vibrations of cylindrical structures. In *Proc. 1st Australian Conf. on Hydraul. and Fluid Mech.* (ed. R. Silvester), pp. 213–239. Pergamon.

Wardlaw, R. L. & Cooper, K. R. 1973 A wind tunnel investigation of the steady aerodynamic forces on smooth and stranded twin bundled power conductors for the Aluminium Company of America. *Natl Aero. Estab., Canada,* LTR-LA-117.

WAWZONEK, M. A. & PARKINSON, G. V. 1979 Combined effects of galloping instability and vortex-resonance. In *Proc. 5th Intl Conf. on Wind Engng, Fort Collins, Colorado*, vol. 2, pp. 673–684.

YANG, C. I. & MORAN, T. J. 1979 Calculations of added mass and damping coefficients for hexagonal cylinders in a confined viscous fluid. In *Flow-Induced Vibrations* (ed. S. S. Chen & M. D. Bernstein), pp. 97–103. ASME.

ZDRAVKOVICH, M. M. 1974 Flow induced vibrations of two cylinders in tandem, and their suppression. In *Proc. Intl Symp. Flow Induced Structural Vibrations, Karlsruhe 1972*, pp. 631–639. Springer.

ZDRAVKOVICH, M. M. 1977 Review of flow interference between two circular cylinders in various arrangements. *Trans. ASME* I: *J. Fluids Engng* **99**, 618–633.

ZDRAVKOVICH, M. M. 1982 Flow-induced oscillation of two interfering circular cylinders. In *Intl Conf. on Flow-Induced Vibrations in Fluid Engng, Reading, England*, pp. 141–154.